Intensity of Singular Stress Field over the Entire Bond Line Thickness Range Useful for Evaluating the Adhesive Strength for Plate and Cylinder Butt Joints

Nao-Aki Noda[1], Fei Ren[1], Rei Takaki[1], Zefeng Wang[1], Kazuhiro Oda[2], Tatsujiro Miyazaki[3], and Yoshikazu Sano[1]

1. Kyushu Institute of Technology, 1-1, Sensui-cho, Tobata-Ku, Kitakyushu-Shi, Fukuoka, Japan
2. Oita University, 700 Dannoharu, Oita-Shi, Oita, Japan
3. University of the Ryukyus, 1 Senbaru, Nishihara, Nakagami, Okinawa 903-0213, Japan

*Corresponding author: Nao-Aki NODA,
Department of Mechanical Engineering, Kyushu Institute of Technology, 1-1 Sensui-cho, Tobata-ku, Kitakyushu-shi, Fukuoka 804-8550, Japan,
TEL&FAX: +81-93-884-3124, E-mail: noda@mech.kyutech.ac.jp

Abstract: Our previous research has indicated that the bonded strength can be expressed in terms of the intensity of the singular stress field (ISSF). Since the ISSF is quite useful for evaluating the bonded strength, in this study, the variation of the ISSF is investigated over the entire bondline thickness range of plate and cylinder butt joints. Here, an effective mesh-independent technique combined with a standard FEM approach is used to obtain the ISSFs under arbitrary material combinations. A reference solution of simply bonded plate is used to eliminate FEM error since the exact ISSF is available. This paper clarifies the differences between the fracture behaviors of the bonded plate and cylindrical butt joints.

Key Words: Adhesive joint, Debonding, Intensity of Singular Stress Field, Finite Element Method, Fracture Mechanics

Nomenclature

E	Young's modulus
$e_{\min}$	Minimum element size
F_σ^C	ISSF of bonded cylinder normalized by W, $= K_\sigma^C/\sigma W^{1-\lambda}$
F_σ^{C*}	ISSF of bonded cylinder normalized by h, $= K_\sigma^C/\sigma h^{1-\lambda}$

F_σ^P	ISSF of bonded plate normalized by *W*, $= K_\sigma^P/\sigma W^{1-\lambda}$
F_σ^{P*}	ISSF of bonded plate normalized by *h*, $= K_\sigma^P/\sigma h^{1-\lambda}$
G	Shear modulus
K_σ^C	ISSF for bonded cylinder
K_σ^P	ISSF for bonded plate
$K_{\sigma c}$	Critical ISSF at debonding fracture
h	Bondline thickness
r	Distance from the interface end
u_{r0}^{CYL}	Real radial displacement of bonded cylinder
W	Plate width and radius of bonded cylinder
α, β	Dundurs' parameters
$\varepsilon_{j0,FEM}^C, \gamma_{rz0,FEM}^C$	FEM strain of bonded cylinder at interface end
$\varepsilon_{i0,FEM}^P, \gamma_{xy0,FEM}^P$	FEM strain of bonded plate at interface end
θ	Angle from the corner on the interface
λ	Singular index
ν	Poisson's ratio
σ_c	Adhesive tensile strength
$\sigma_j^C,\ \tau_{rz}^C$	Real stress of bonded cylinder
$\sigma_i^P,\ \tau_{xy}^P$	Real stress of bonded plate
$\sigma_{i0,FEM}, \tau_{xy0,FEM}$	FEM stress at interface end
$\sigma_{j0,FEM}^C, \tau_{rz0,FEM}^C$	FEM stress of bonded cylinder at interface end
$\sigma_{i0,FEM}^P, \tau_{xy0,FEM}^P$	FEM stress of bonded plate at interface end
$\tilde{\sigma}_{j0,FEM}^C, \tilde{\tau}_{rz0,FEM}^C$	Non-singular FEM stress of bonded cylinder at interface end
σ^{real}	Real stress at interface end
$\sigma_y^\infty,\ \sigma_z^\infty$	Uniform applied stress

1. Introduction

Adhesive joints are widely used in numerous industrial sectors, such as automobile, shipbuilding and aeronautics [1-3]. Compared with the other traditional joints, adhesive joints have advantages of light weight, low cost and

easy to process. However, different material properties cause singular stress at the interface end, which may lead to debonding failure in structures[4-12]. The bonded strength can be expressed in terms of the intensity of the singular stress field (ISSF). The ISSF K_σ and the normalized ISSF F_σ can be determined from the interface stress as shown in Eq. (1) [13, 14] by using the local polar coordinate (r,θ) indicated in Fig.1 (a), (b).

$$ISSF\ K_\sigma = \lim_{r\to 0}\left[r^{1-\lambda} \times \sigma_\theta(r)\big|_{\theta=\pi/2} \right], \quad Normalized\ ISSF\ F_\sigma = \frac{K_\sigma}{\sigma\, W^{1-\lambda}} \tag{1}$$

Since the singular index $\lambda \neq 0.5$ different from the singular index for cracks

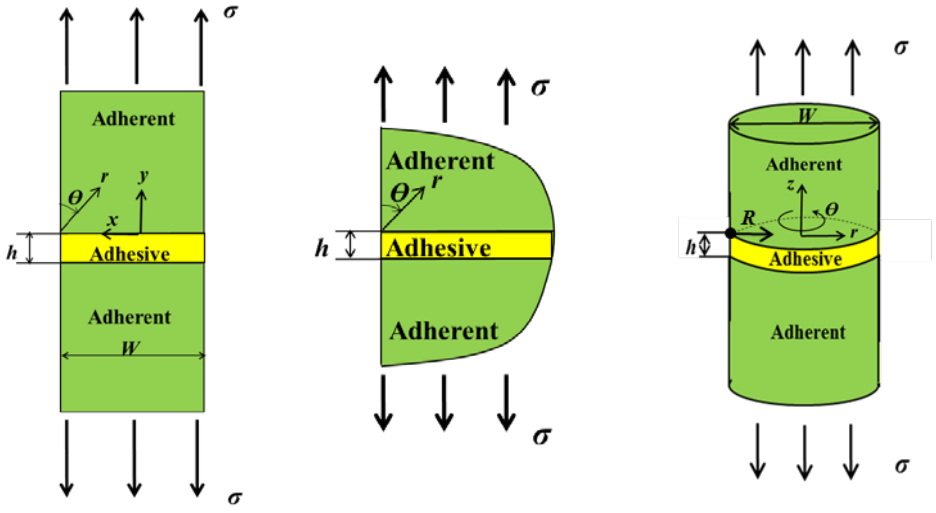

(a) Plate butt joint (b) Semi-infinite butt joint (c) Cylinder butt joint

Fig.1. Adhesive butt joints (Fig.1(b) is equivalent to Fig.1(a) when $h/W \leq 0.01$ in Fig.1(a))

$\lambda = 0.5$, the term ISSF (=Intensity of Singular Stress Field) is used instead of SIF (=Stress Intensity Factor) usually used for cracks generally.

Fig.2 (a) shows the adhesive joint strength for plate butt joint expressed as the critical remote tensile stress σ_c [15]. It is known that the debonding stress increases with decreasing the adhesive thickness [15-19]. In Ref. [19], the effect of joint component mechanical properties and adhesive layer thickness on stress concentration was discussed for a bonded cylindrical specimen. In Ref. [7-9] the ISSF is considered under arbitrary material combinations for h/W=0.1 and 0.001. Our previous studies have indicated that the normalized ISSF decreases with decreasing the bondline thickness as shown in Fig. 2(b) under tension [7] and under bending [8, 9]. From the critical remote tensile stress shown in Fig. 2(a), (b), the critical ISSF can be calculated when the debonding occurs. As shown in Fig. 3, the debonding strength can be expressed as a constant value of ISSF [12, 20].

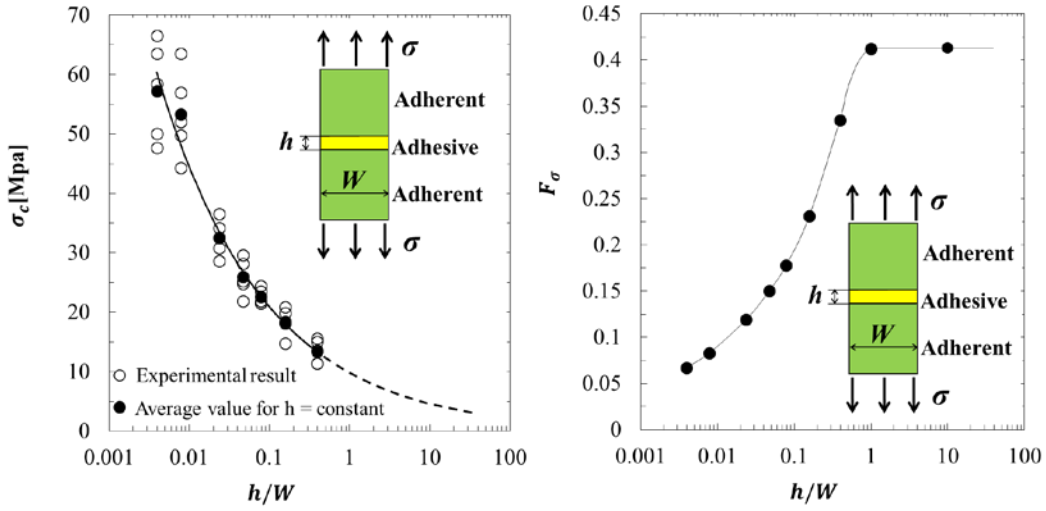

(a) Critical remote tensile stress σ_c [15] (b) Normalized ISSF F_σ under constant σ [12]

Fig. 2 Relationship between critical remote tensile stress σ_c, normalized ISSF F_σ and bondline thickness h

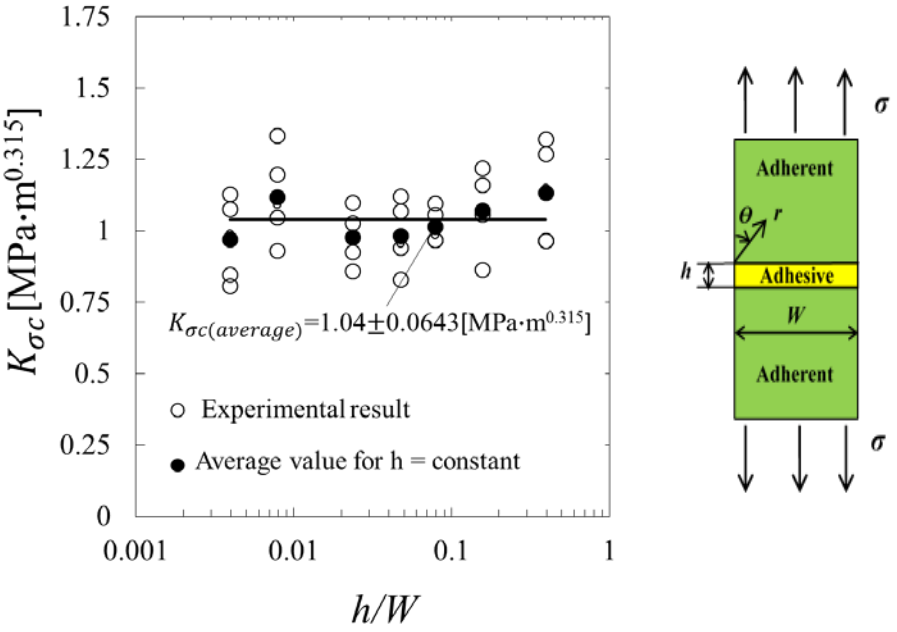

Fig.3 Relationship between $K_{\sigma c}$ and h[12]

From the above discussion, it is seen that the solution for ISSF shown in Fig. 2(b) is quite useful for evaluating the adhesive strength. For large adhesive thickness h, the normalized ISSF F_σ becomes constant as shown in Fig. 2(b), and therefore can be estimated easily for any material combibation (see Appendix A [14]). However, for small bondline thickness h, which is necessary for evaluating normal adhesive layers, the normalized ISSF F_σ decreases with decreasing h and does not become constant. In this paper, therefore, the ISSF vs. h relation will be clarified mainly focusing on the small adhesive thickness. As a three-dimensional fundamental solution, the cylindrical butt joint in Fig. 1(c) is also considered to be compared with plate butt joint. The aim of this paper is to provide the solutions of ISSFs useful for evaluating the adhesive joint strength. In this study, arbitrary material combinations will be considered for the future use of adhesive joint in wide engineering fields.

2. Mesh-independent technique to evaluate the ISSF of plate butt joint

In this section, a mesh-independent technique will be explained for the readers to understand how to obtain accurate ISSFs although similar methods have been used in [9, 12, 20]. In the first place, a plate butt joint as shown in Fig. 1(a) is considered. When the bondline thickness h is significantly less than the

adhesive width $W(h/W \to 0)$, the solution may be regarded as the bonded semi-infinite plate as shown in Fig. 1(b). It is known that the interface stress $\sigma_{ij}(ij = rr, r\theta, \theta\theta)$ at the edge can be expressed in the form $\sigma_{ij} \propto 1/r^{1-\lambda}$ when $\alpha(\alpha - 2\beta) > 0$. Notations α and β denote Dundurs' parameters [21] expressed by Poisson's ratio v and shear modulus G, and notation λ denotes the singular index at the interface expressed as the root of the following equations [22, 23].

$$\left[\sin^2\left(\frac{\pi}{2}\lambda\right) - \lambda^2\right]^2 \beta^2 + 2\lambda^2\left[\sin^2\left(\frac{\pi}{2}\lambda\right) - \lambda^2\right]\alpha\beta + \lambda^2\left[\lambda^2 - 1\right]\alpha^2 + \frac{\sin^2(\lambda\pi)}{4} = 0 \tag{2}$$

$$\alpha = \frac{G_1(\kappa_2 + 1) - G_2(\kappa_1 + 1)}{G_1(\kappa_2 + 1) + G_2(\kappa_1 + 1)} \qquad \beta = \frac{G_1(\kappa_2 - 1) - G_2(\kappa_1 - 1)}{G_1(\kappa_2 + 1) + G_2(\kappa_1 + 1)} \tag{3}$$

$$\kappa_j = \begin{cases} \dfrac{3 - \nu_j}{1 + \nu_j} \left(\textit{plane stress}\right) \\ 3 - 4\nu_j \left(\textit{plane strain}\right) \end{cases} \left(j = 1, 2\right) \tag{4}$$

The ISSF K_σ at the adhesive dissimilar joint end is defined from the real interface stress σ_y^{real} as shown in equation (5).

$$ISSF\ K_\sigma = \lim_{r \to 0}\left[r^{1-\lambda}\sigma_y^{real}(r)\right],\ \text{but}\ \ ISSF\ K_\sigma \neq \lim_{r \to 0}\left[r^{1-\lambda}\sigma_y^{FEM}(r)\right] \tag{5}$$

However, the ISSF cannot be easily determined by FEM since real interface singular stress σ_y^{real} is different from the FEM stress σ_y^{FEM}, which is largely depending on the mesh size. In the previous papers [8, 9, 12], therefore, the FEM stress ratio $\sigma_y^{FEM} / \sigma_{y(\mathrm{Re}\,f)}^{FEM}$ was considered by using a reference problem which has been solved very accurately in the previous study. It should be noted that the FEM stress ratio of the unknown reference problems is independent of the mesh size if the same FEM mesh is applied. This is because the FEM errors of two problems are nearly the same. As the reference solution, a simply bonded plate can be used since the ISSF has been analysed very accurately by using the body force method [14] (see Appendix A). Since the FEM stress ratio and the reference solution are very accurate, the new results also can be obtained very accurately.

In this study, the ISSF of a simply bonded plate will be used as the reference problem, as is shown in Equation (6).

$$\frac{K_\sigma}{K_{\sigma(\mathrm{Ref.})}} = \lim_{r\to 0}\frac{\left[r^{1-\lambda}\sigma_y^{real}\right]}{\left[r^{1-\lambda}\sigma_{y(\mathrm{Ref.})}^{real}\right]} = \lim_{r\to 0}\frac{\sigma_y^{FEM}}{\sigma_{y(\mathrm{Ref.})}^{FEM}} \qquad (6)$$

Here, the subscript (Ref.) denotes the ISSF or the stress for reference problem.

The finite element analysis is carried out for the butt joints by using the commercial software ANSYS 16.2. Fig. 4 (a), (b) shows the FEM mesh for the butt joint for *h/W*=0.001 and the bonded plate for *h/W*=1. Because of symmetry, quarter models are considered for analysis. The finite-element mesh consists of two-dimensional four-node element named PLANE42 and finer subdivisions are used around the interface end. As shown in Figure 4 (b), the same mesh division pattern is used to eliminate FEM error. The total number of elements have to be larger if the adhesive layer is thin since the interaction between the two interface ends becomes larger. Therefore, the total number of elements 196794 is necessary for *h/W*=0.001, but the total number of elements 2560 is enough for *h/W*=1. Table 1 shows an example of stress ratio for the butt joint over the bonded plate by using the mesh in Fig.4 with different minimum mesh sizes e_{min}. In Table 1 it should be noted that $\sigma_y^{\mathrm{mat1}}=\sigma_y^{\mathrm{mat2}}$, $\tau_{xy}^{\mathrm{mat1}}=\tau_{xy}^{\mathrm{mat2}}$ but $\sigma_x^{\mathrm{mat1}} \neq \sigma_x^{\mathrm{mat2}}$, $\sigma_z^{\mathrm{mat1}} \neq \sigma_z^{\mathrm{mat2}}$ at the interface. Here $\sigma_{ij}^{\mathrm{mat1}}$ denotes the stress for matrial 1 and $\sigma_{ij}^{\mathrm{mat2}}$ denotes the stress for matrial 2.

As shown in Table 1, however, all the stress components ratios $\sigma_{ij}^{P}/\sigma_{ij}^{REF}$ are continuous across the interface and coincide with each other. The results are independent of the element size when the mesh independent technique is employed by using the same FEM mesh pattern.

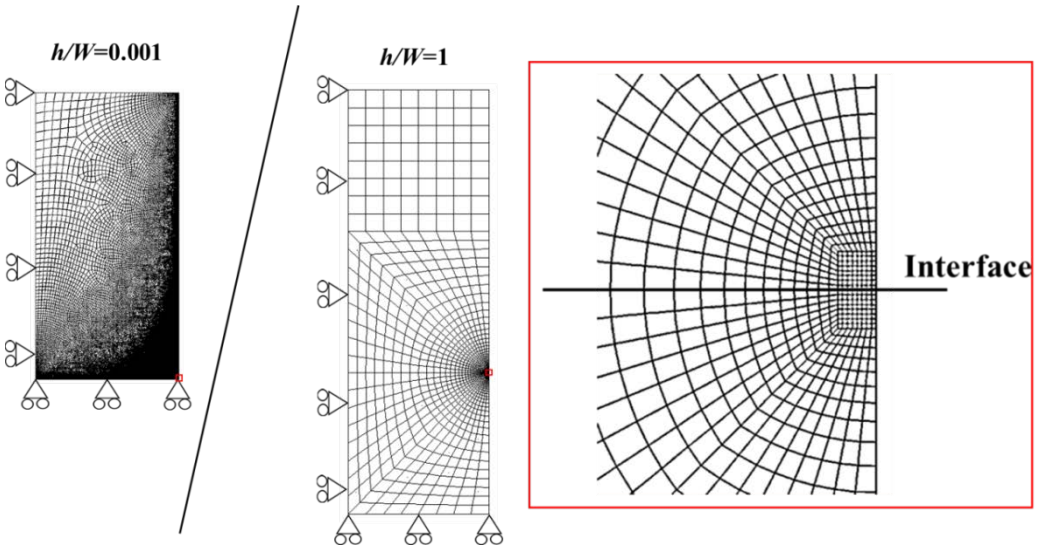

(a) FEM model

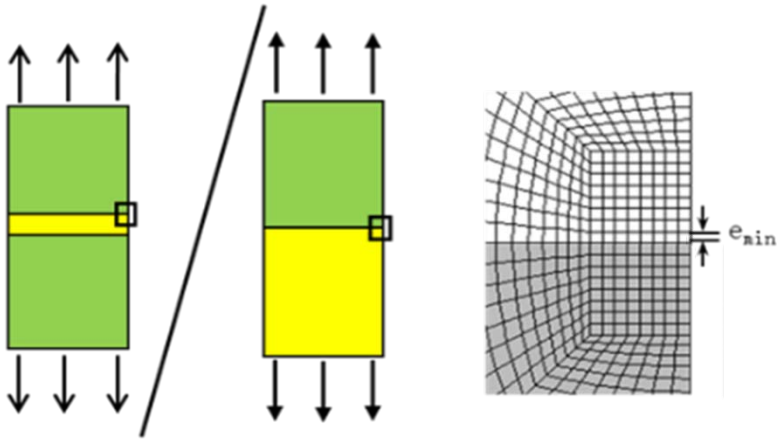

(b) Detail around the interface end

Fig.4 FEM mesh for the plate butt joint *h/W*=0.001 and simply bonded plate *h/W*=1

Table 1 Mesh-independent FEM stress ratio $\sigma^{P}_{ij0,FEM}/\sigma^{REF}_{ij0,FEM}$ when E_1=1000,ν_1=0.23, E_2=105.06,ν_2=0.32,*h/W*=0.001

	$\sigma^{P}_{x0,FEM}/\sigma^{REF}_{x0,FEM}$		$\sigma^{P}_{y0,FEM}/\sigma^{REF}_{y0,FEM}$		$\sigma^{P}_{z0,FEM}/\sigma^{REF}_{z0,FEM}$		$\tau^{P}_{xy,FEM}/\tau^{REF}_{xy,FEM}$	
Material	Mat.1	Mat.2	Mat.1	Mat.2	Mat.1	Mat.2	Mat.1	Mat.2
e_{min} =2.5^{-15}	0.3604	0.3603	0.3604		0.3604	0.3604	0.3603	
e_{min} =2.5^{-18}	0.3604	0.3604	0.3604		0.3604	0.3604	0.3603	

2. Effect of bond line thickness on the ISSF for plate butt joint

In the previous papers [7-9, 20] for the plate butt joint as shown in Fig.1 (a), the normalized ISSF for bonded plate F^{P}_{σ} was defined in Equation (7).

$$\text{Normalized ISSF } F_\sigma^P = K_\sigma^P/\sigma W^{1-\lambda}. \quad (7)$$

In Equation (7), the ISSF for bonded plate K_σ^P is normalized in terms of the remote tensile stress σ and the plate width W. This is because the ISSF is controlled by the width W. Namely, if W becomes larger, the ISSF becomes larger.

However, if the bondline thickness h is small, the width W does not affect the ISSF K_σ^P anymore. Consider a small adhesive thickness joint as shown in Fig.1 (b), which has two singular poits at the two interface ends. If h becomes smaller, the interaction between two interface ends becomes larger. Therefore, the ISSF is controlled by h instead of W, and therefore the ISSF K_σ^P should be normalized by h instead of W. In other words, for small h, the butt joint in Fig.1 (a) can be regarded as the bonded semi-infinite plate as shown in Fig.1 (b). In this case, the ISSF K_σ^P in Fig. 1 (b) should be normalized in terms of the remote tensile stress σ and the adhesive thickness h as shown in Equation (8).

$$\text{Normalized ISSF } F_\sigma^{P*} = K_\sigma^P/\sigma h^{1-\lambda}. \quad (8)$$

Table 2 shows F_σ^P values and normalized value of $F_\sigma^P/F_\sigma^P|_{h/W\to\infty}$. Fig.5 shows F_σ^P vs. *h/W* relation for several material combinations. As shown in Table 2 and Fig.5, when $h/W \geq 1$, the normalized ISSFs F_σ^P are always the same. This is due to Saint'-Venant's Principle stating that the effects of two different but statically equivalent loads are the same at sufficiently large distances from load, that is, $h/W \geq 1$. As shown in Table 2, the normalized ISSF F_σ^P has the same value in the range $h/W \geq 1$ since the thickness effect can be negligible.

Table 3 shows F_σ^{P*} values and Fig.6 shows F_σ^{P*} vs. *h/W* relation. It is seen that when the bondline thickness is small, the F_σ^{P*} value always becomes constant. The plate butt joint in Fig.1 (a) can be regarded as a bonded semi-infinite plate in Fig.1 (b) when the relative bondline thickness $h/W \leq 0.01$. From Fig.5 and Fig.6, it is found that $F_\sigma^{P*} = K_\sigma^P/\sigma h^{1-\lambda}$ is more suitable for small h since F_σ^{P*} is insensitive to h/W compared to $F_\sigma^P = K_\sigma^P/\sigma W^{1-\lambda}$. As shown in Table 3, the normalized ISSF F_σ^{P*} has almost the same value in the range $h/W \leq 0.01$ within 0.6% deviation and in the range $h/W \leq 0.1$ within 10% deviation since the width effect is smaller.

Table 4 and Fig. 7 show the normalized ISSFs F_σ^{P*} under arbitrary material combinations useful for $h/W \leq 0.01$ and within 10% error for $h/W \leq 0.1$. Since the solution for bonded plate $h/W \geq 1.0$ is indicated in Appendix A, the accurate

results can be obtained by the interpolation in the range for $0.01 \leq h/W \leq 1.0$ under arbitrary material combination.

Table 2 F_σ^P and $F_\sigma^P / F_\sigma^P|_{h/W\to\infty}$ of butt joint with varying the bondline thickness

F_σ^P						
h/W \ (α,β)	(0.3,0)	(0.4,-0.1)	(0.4,0)	(0.4,0.1)	(0.5,-0.1)	(0.5,0)
0.001	0.416	0.152	0.275	0.490	0.095	0.173
0.002	0.435	0.167	0.295	0.511	0.107	0.191
0.005	0.462	0.188	0.324	0.540	0.126	0.219
0.01	0.484	0.208	0.349	0.563	0.144	0.244
0.05	0.545	0.267	0.421	0.627	0.199	0.316
0.1	0.582	0.306	0.464	0.662	0.236	0.361
0.5	0.745	0.538	0.659	0.787	0.473	0.573
1	0.794	0.612	0.716	0.821	0.548	0.633
10	0.796	0.615	0.718	0.822	0.551	0.635
→∞	0.796	0.615	0.718	0.822	0.551	0.635
$F_\sigma^P / F_\sigma^P|_{h/W\to\infty}$						
h/W \ (α,β)	(0.3,0)	(0.4,-0.1)	(0.4,0)	(0.4,0.1)	(0.5,-0.1)	(0.5,0)
0.001	0.523	0.247	0.383	0.596	0.172	0.272
0.002	0.546	0.272	0.411	0.622	0.194	0.301
0.005	0.580	0.306	0.451	0.657	0.229	0.345
0.01	0.608	0.338	0.486	0.685	0.261	0.384
0.05	0.685	0.434	0.586	0.763	0.361	0.498
0.1	0.731	0.498	0.646	0.805	0.428	0.569
0.5	0.936	0.875	0.918	0.957	0.858	0.902
1	0.997	0.995	0.997	0.999	0.995	0.997
10	1.000	1.000	1.000	1.000	1.000	1.000
→∞	1.000	1.000	1.000	1.000	1.000	1.000

Table 3 F_σ^{P*} and $F_\sigma^{P*} / F_\sigma^{P*}|_{h/W\to 0}$ of butt joint with varying adhesive thickness

F_σ^{P*}						
h/W \ (α,β)	(0.3,0)	(0.4,-0.1)	(0.4,0)	(0.4,0.1)	(0.5,-0.1)	(0.5,0)
→0	0.643	0.384	0.558	0.740	0.326	0.476
0.001	0.643	0.384	0.558	0.740	0.326	0.476
0.002	0.643	0.384	0.558	0.740	0.326	0.476
0.005	0.644	0.384	0.558	0.740	0.327	0.477
0.01	0.646	0.386	0.560	0.742	0.328	0.479
0.05	0.658	0.399	0.572	0.750	0.340	0.491
0.1	0.672	0.417	0.588	0.759	0.357	0.507
0.5	0.778	0.590	0.707	0.821	0.536	0.634
1	0.794	0.612	0.716	0.821	0.548	0.633
10	0.689	0.451	0.567	0.716	0.365	0.453
$F_\sigma^{P*} / F_\sigma^{P*}|_{h/W\to 0}$						
h/W \ (α,β)	(0.3,0)	(0.4,-0.1)	(0.4,0)	(0.4,0.1)	(0.5,-0.1)	(0.5,0)
→0	1.000	1.000	1.000	1.000	1.000	1.000
0.001	1.000	1.000	1.000	1.000	1.000	1.000
0.002	1.000	1.000	1.000	1.000	1.000	1.000
0.005	1.002	1.000	1.000	1.000	1.003	1.002
0.01	1.005	1.005	1.004	1.003	1.006	1.006

0.05	1.023	1.039	1.025	1.014	1.043	1.032
0.1	1.045	1.086	1.054	1.026	1.095	1.065
0.5	1.210	1.536	1.267	1.109	1.644	1.332
1	1.235	1.594	1.283	1.109	1.681	1.330
10	1.072	1.174	1.016	0.968	1.120	0.952

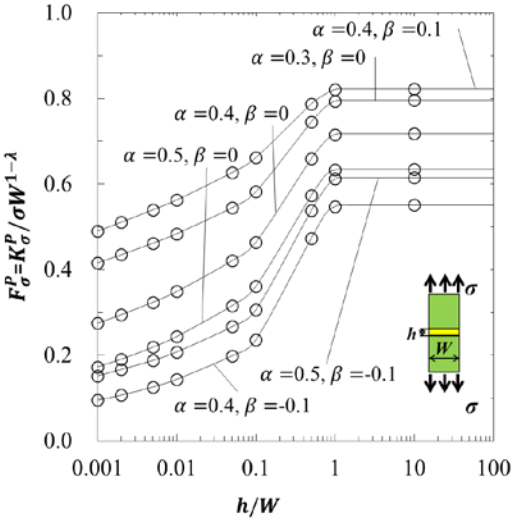

Fig.5. F_σ^P is constant when $h/W \geq 1.0$

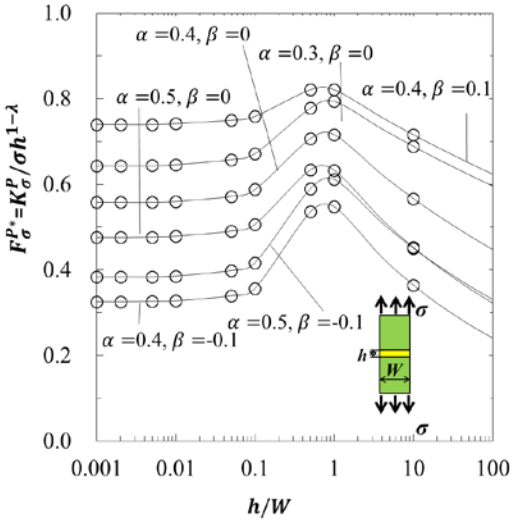

Fig.6. F_σ^{P*} is constant when $h/W \leq 0.01$

Table 4 Normalized ISSF F_σ^{P*} of a semi-infinite butt joint in Fig.1 (b)

$$F_\sigma^{P*} = K_\sigma^P / \sigma h^{1-\lambda}$$

	β=-0.4	β=-0.3	β=-0.2	β=-0.1	β=0	β=0.1	β=0.2	β=0.3	β=0.4
α=-1	1.134	1.209	1.315	1.404	1.498				
α=-0.9	1.066	1.148	1.252	1.347	1.424				
α=-0.8	1.000	1.082	1.191	1.289	1.352				
α=-0.7	0.904	1.032	1.134	1.223	1.288				
α=-0.6		0.990	1.075	1.156	1.227	1.420			
α=-0.5		0.946	1.028	1.119	1.185	1.360			
α=-0.4		0.901	1.000	1.092	1.166	1.320			
α=-0.3		0.812	0.940	1.057	1.142	1.280			
α=-0.2		0.680	0.837	1.000	1.113	1.250	1.500		
α=-0.1			0.710	0.916	1.061	1.230	1.460		
α=0			0.585	0.799	1.000	1.195	1.430		
α=0.1			0.460	0.654	0.873	1.124	1.380		
α=0.2			0.353	0.550	0.758	1.000	1.314	1.918	
α=0.3				0.456	0.643	0.858	1.181	1.769	
α=0.4				0.384	0.558	0.740	1.000	1.572	
α=0.5				0.326	0.476	0.630	0.813	1.293	
α=0.6				0.257	0.405	0.546	0.686	1.000	
α=0.7					0.340	0.470	0.588	0.794	1.730
α=0.8					0.290	0.403	0.506	0.634	1.000
α=0.9					0.223	0.333	0.430	0.543	0.746
α=1					0.169	0.265	0.358	0.456	0.495

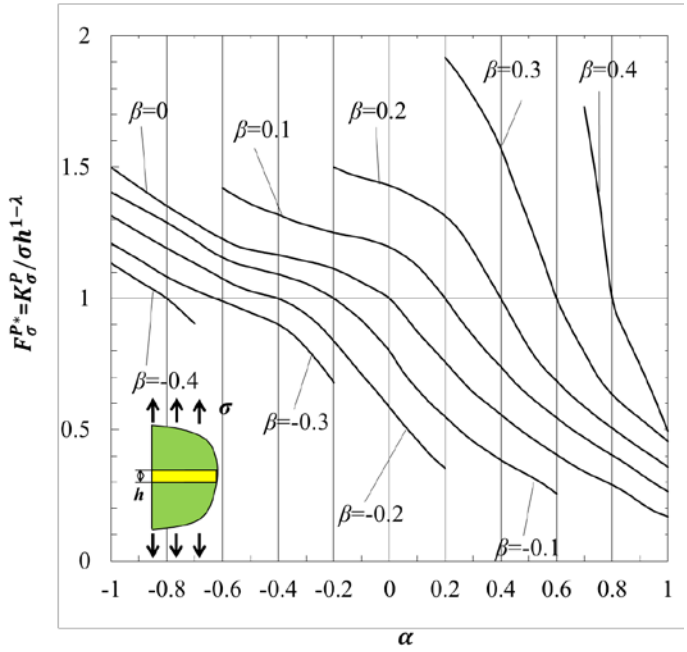

Fig.7 Normalized ISSF F_σ^{P*} of a semi-infinite butt joint in Fig.1 (b) which is useful for $h/W \leq 0.01$ in Fig.1(a)

3. **Mesh-independent technique to evaluate the ISSF of cylindrical butt joint**

In this section, the mesh-independent technique will be explained for the readers to understand how to obtain accurate ISSFs for cylindrical butt joints although the similar method was used to analyze bonded cylinder and bonded pipe in [24]. The ISSF of a semi-infinite butt joint K_σ^P has been analyzed in the previous section. To obtain the ISSF of cylindrical butt joint K_σ^C, the new results of K_σ^P can be used as the reference solution. Table 5 shows an example of stress ratio for the cylindrical butt joint in Fig.1 (c) over the semi-infinite butt joint in Fig. 1(a). Different ftom Table 1, the ratios of stress components are not always consistent with each other even though the same FE mesh is applied. It should be noted that the value of $\sigma_{\theta 0,FEM}^C/\sigma_{z0,FEM}^P$ is quite different from other stress ratios. Therefore, we have to consider the mesh-independent technique for axi-symmetric problems in some special aspects.

Table 5 Ratio of $\sigma_{ij0,FEM}^C/\sigma_{ij0,FEM}^P$
(E_1=1000,ν_1=0.23, E_2=105.06,ν_2=0.32,h/W=0.001)

	$\sigma_{r0,FEM}^C/\sigma_{x0,FEM}^P$		$\sigma_{z0,FEM}^C/\sigma_{y0,FEM}^P$		$\sigma_{\theta 0,FEM}^C/\sigma_{z0,FEM}^P$		$\tau_{rz,FEM}^C/\tau_{xy,FEM}^P$	
Material	Mat. 1	Mat. 2	Mat. 1	Mat. 2	Mat. 1	Mat. 2	Mat. 1	Mat. 2
$e_{\min}=2.5^{-15}$	0.9937	0.9937	0.9955		0.5679	0.9745	0.9937	

$e_{min}=2.5^{-18}$	0.9937	0.9937	0.9949	0.7187 0.9813	0.9937

The difference between Table 1 and Table 5 can be explained in the following way. For the plane strain problem as shown in Fig. 1(a), the strain in the z-direction is zero. While for the axi-symmetric problem as shown in Fig. 1(c), the strain in the θ direction on the outer cylinder surface can be expressed as [25]:

$$\varepsilon_\theta = \frac{u_r}{(W/2)},$$

which can lead to non-zero stresses [24, 26]. Then the stress of the unknown problem shown in Fig. 1(c) is expressed as:

$$\sigma_j^C = \frac{K_{\sigma_j}^C}{R^{1-\lambda}} + \sigma_j^0 = \hat{\sigma}_j^C + \sigma_j^0 \ (j = r, z, \theta), \quad \tau_{rz}^C = \frac{K_{\tau_{xy}}^C}{R^{1-\lambda}} + \tau_{rz}^0 = \hat{\tau}_{rz}^C + \tau_{rz}^0. \tag{9}$$

where R is the local distance from the axisymmetric interface end.

In Equation (9), the first terms $\hat{\sigma}_j^C$ and $\hat{\tau}_{rz}^C$ denote singular stress and the second terms $\tilde{\sigma}_j^C$ and $\tilde{\tau}_{rz}^C$ denote non-singular stress[26-28] as

$\left(\sigma_{r0}^C\right)^{\text{mat1}}, \left(\sigma_{z0}^C\right)^{\text{mat1}}, \left(\sigma_{\theta 0}^C\right)^{\text{mat1}}, \left(\tau_{rz}^0\right)^{\text{mat1}}$ in material 1;

$\left(\sigma_{r0}^C\right)^{\text{mat2}}, \left(\sigma_{z0}^C\right)^{\text{mat2}}, \left(\sigma_{\theta 0}^C\right)^{\text{mat2}}, \left(\tau_{rz}^0\right)^{\text{mat2}}$ in material 2.

These eight stress components should satisfy the boundary conditions for bonded interface and free edge of the outer surface as well as the compatibility condition. As a result, they are reduced to the following equations.

$$\left(\sigma_{r0}^C\right)^{\text{mat1}} = \left(\sigma_{r0}^C\right)^{\text{mat2}} = \left(\tau_{rz}^0\right)^{\text{mat1}} = \left(\tau_{rz}^0\right)^{\text{mat2}} = 0 \tag{10}$$

$$\left(\sigma_{z0}^C\right)^{\text{mat1}} = \left(\sigma_{z0}^C\right)^{\text{mat2}} = \sigma_{z0}^C \tag{11}$$

$$\left(\varepsilon_{\theta 0}^0\right)^{\text{mat1}} = \left(\varepsilon_{\theta 0}^0\right)^{\text{mat2}} = \varepsilon_{\theta 0}^0 \tag{12}$$

$$\left(\varepsilon_{r0}^0\right)^{\text{mat1}} = \left(\varepsilon_{r0}^0\right)^{\text{mat2}} = \varepsilon_{r0}^0 \tag{13}$$

By substituting Eqs. (10), (11) into Eq. (12), we have

$$\left(\varepsilon_{\theta 0}^0\right)^{\text{mat1}} - \left(\varepsilon_{\theta 0}^0\right)^{\text{mat2}} = \frac{1}{E_1}\left[\left(\sigma_{\theta 0}^C\right)^{\text{mat1}} - \nu_1\left(\sigma_{z0}^C\right)^{\text{mat1}}\right] - \frac{1}{E_2}\left[\left(\sigma_{\theta 0}^C\right)^{\text{mat2}} - \nu_2\left(\sigma_{z0}^C\right)^{\text{mat2}}\right] = 0.$$

Thus

$$\left(\frac{\nu_1}{E_1} - \frac{\nu_2}{E_2}\right)\sigma_{z0}^C = \frac{\left(\varepsilon_{\theta 0}^0\right)^{\text{mat1}}}{E_1} - \frac{\left(\varepsilon_{\theta 0}^0\right)^{\text{mat2}}}{E_2} \tag{14}$$

Similarly, for Eq. (13), we have

$$\left(\varepsilon_{r0}^{C}\right)^{\text{mat1}}-\left(\varepsilon_{r0}^{C}\right)^{\text{mat2}}=\frac{1}{E_1}\left[\left(\sigma_{r0}^{C}\right)^{\text{mat1}}-\nu_1\left(\sigma_{z0}^{C}\right)^{\text{mat1}}\right]-\frac{1}{E_2}\left[\left(\sigma_{\theta 0}^{C}\right)^{\text{mat2}}-\nu_2\left(\sigma_{z0}^{C}\right)^{\text{mat2}}\right]=0\,.$$

Substitute Eq. (14) into the above equation, we have

$$\frac{\left(\sigma_{\theta 0}^{C}\right)^{\text{mat1}}}{\left(\sigma_{\theta 0}^{C}\right)^{\text{mat2}}}=\frac{1+\nu_2}{1+\nu_1}\cdot\frac{E_1}{E_2}\,. \tag{15}$$

From Eq. (14) and Eq. (15) we can obtain

$$\frac{\left(\sigma_{\theta 0}^{C}\right)^{\text{mat1}}}{\sigma_{z0}^{C}}=-\frac{\nu_1-\frac{E_1}{E_2}\nu_2}{\frac{\nu_1-\nu_2}{1+\nu_2}}\,. \tag{16}$$

And

$$\frac{\left(\sigma_{\theta 0}^{C}\right)^{\text{mat2}}}{\sigma_{z0}^{C}}=-\frac{\nu_2-\frac{E_2}{E_1}\nu_1}{\frac{\nu_2-\nu_1}{1+\nu_2}}\,. \tag{17}$$

For axis symmetric problem under cylindrical coordinate system, there is

$$\begin{cases}\varepsilon_r=\dfrac{\partial u_r}{\partial r}\\ \varepsilon_\theta=\dfrac{u_r}{r}\\ \gamma_{rz}=\dfrac{\partial u_r}{\partial z}+\dfrac{\partial u_z}{\partial r}\end{cases} \tag{18}$$

Recall Eq. (12) we can obtain:

$$\begin{aligned}&\left(\varepsilon_{\theta 0}^{C}\right)^{\text{mat1}}=\left(\varepsilon_{\theta 0}^{C}\right)^{\text{mat2}}=\varepsilon_{\theta 0}^{C}=\varepsilon_\theta=\frac{u_r}{r}\\ &=\frac{1}{E_1}\left\{\left(\sigma_{\theta 0}^{C}\right)^{\text{mat1}}-\nu_1\left[\left(\sigma_{r0}^{C}\right)^{\text{mat1}}+\left(\sigma_{z0}^{C}\right)^{\text{mat1}}\right]\right\}\\ &=-\frac{\left(1+\nu_1\right)\nu_1E_2-\left(1+\nu_2\right)\nu_2E_1}{\left(\nu_1-\nu_2\right)E_1E_2}\sigma_{z0}^{C}\end{aligned}$$

Thus

$$\begin{aligned}&\left(\sigma_{z0}^{C}\right)^{\text{mat1}}=\left(\sigma_{z0}^{C}\right)^{\text{mat2}}=\sigma_{z0}^{C}\\ &=-\frac{\left(\nu_1-\nu_2\right)E_1E_2}{\left(1+\nu_1\right)\nu_1E_2-\left(1+\nu_2\right)\nu_2E_1}\frac{u_r}{r}\\ &=-\frac{\left(\nu_1-\nu_2\right)E_1E_2}{\left(1+\nu_1\right)\nu_1E_2-\left(1+\nu_2\right)\nu_2E_1}\frac{u_{r0}^{C}}{(W/2)}\end{aligned} \tag{19}$$

Substituting Eq. (19) into Eqs. (16), (17) gives

$$\left(\sigma_{\theta 0}^{C}\right)^{\text{mat1}} = \frac{(1+\nu_2)(\nu_1 E_2 - \nu_2 E_1)E_1}{(1+\nu_1)\nu_1 E_2 - (1+\nu_2)\nu_2 E_1} \frac{u_{r0}^{C}}{(W/2)} \tag{20}$$

$$\left(\sigma_{\theta 0}^{C}\right)^{\text{mat2}} = \frac{(1+\nu_1)(\nu_1 E_2 - \nu_2 E_1)E_2}{(1+\nu_1)\nu_1 E_2 - (1+\nu_2)\nu_2 E_1} \frac{u_{r0}^{C}}{(W/2)} \tag{21}$$

And recall Eq. (10)

$$\left(\sigma_{r0}^{C}\right)^{\text{mat1}} = \left(\sigma_{r0}^{C}\right)^{\text{mat2}} = \left(\tau_{rz0}^{C}\right)^{\text{mat1}} = \left(\tau_{rz0}^{C}\right)^{\text{mat2}} = 0 \tag{22}$$

The validity of equations (19)-(22) to express non-singular stress components will be discussed in Tables 6, 7, 8. By using the material combination shown in Table 5, Table 6 shows the radial displacement at the interface end, u_{r0}^{C}, and the non-singular stresses which are obtained from Eqs. (19), (20), (21) and (22). Here, displacement u_{r0}^{C} is independent of the element size. Table 7 shows the singular stresses by subtracting the non-singular stresses in Table 6 from the stresses at the interface end. Table 8 shows the ratios of the singular stresses at the interface end of the cylindrical butt joint to those of the semi-infinite butt joint. It is found that the ratio 0.9937 is independent of the element size $e_{\min}$. Since the raio is also independent of the stress components, the validity of (19)-(22) has been confirmed. From the comparison between Table 5 and Table 8, it is seen that $\sigma_{r0,FEM}^{C}$ and $\tau_{rz,FEM}^{C}$ do not have the non-singular stresses because $\tilde{\sigma}_{r0,FEM}^{C} = \tilde{\tau}_{rz0,FEM}^{C} = 0$. The correct ratio of the ISSF can be calculated from $\sigma_{r0,FEM}^{C}$ and $\tau_{rz,FEM}^{C}$ easily since the subtraction process is not necessary.

Table 6 Non-singular stresses of cylindrical butt joint

e_{min}	$\tilde{\sigma}_{r0,FEM}^{C}$		$\tilde{\sigma}_{z0,FEM}^{C}$		$\tilde{\sigma}_{\theta 0,FEM}^{C}$		$\tilde{\tau}_{rz0,FEM}^{C}$		u_{r0}^{C}
	Mat.1	Mat.2	Mat.1	Mat.2	Mat.1	Mat.2	Mat.1	Mat.2	
2.5^{-15}	0.0000	0.0000	0.0065		-0.2616	-0.0255	0.0000		-0.00013153
2.5^{-18}	0.0000	0.0000	0.0065		-0.2616	-0.0255	0.0000		-0.00013154

Table 7 Singular stresses of cylindrical butt joint

e_{min}	$\sigma_{r0,FEM}^{C} - \tilde{\sigma}_{r0,FEM}^{C}$		$\sigma_{z0,FEM}^{C} - \tilde{\sigma}_{z0,FEM}^{C}$		$\sigma_{\theta 0,FEM}^{C} - \tilde{\sigma}_{\theta 0,FEM}^{C}$		$\tau_{rz0,FEM}^{C} - \tilde{\tau}_{rz0,FEM}^{C}$	
	Mat.1	Mat.2	Mat.1	Mat.2	Mat.1	Mat.2	Mat.1	Mat.2
2.5^{-15}	-1.5377	0.9911	4.1917		0.6104	1.3238	0.2144	
2.5^{-18}	-2.3816	1.5356	6.4919		0.9454	2.0503	0.3323	

Table 8 The ratios of singular stresses at the interface e of the cylindrical butt joint and the semi-infinite butt joint

e_{min}	$\dfrac{\sigma_{r0,FEM}^{C} - \tilde{\sigma}_{r0,FEM}^{C}}{\sigma_{x0,FEM}^{P}}$		$\dfrac{\sigma_{z0,FEM}^{C} - \tilde{\sigma}_{z0,FEM}^{C}}{\sigma_{y0,FEM}^{P}}$		$\dfrac{\sigma_{\theta 0,FEM}^{C} - \tilde{\sigma}_{\theta 0,FEM}^{C}}{\sigma_{y0,FEM}^{P}}$		$\dfrac{\tau_{rz0,FEM}^{C} - \tilde{\tau}_{rz0,FEM}^{C}}{\tau_{xy0,FEM}^{P}}$	
	Mat.1	Mat.2	Mat.1	Mat.2	Mat.1	Mat.2	Mat.1	Mat.2
2.5^{-15}	0.9937	0.9937	0.9937		0.9937	0.9937	0.9937	

2.5^{-18}	0.9937	0.9937	0.9937	0.9937	0.9937	0.9937

4. Effect of bondline thickness on the ISSF for cylindrical butt joint

For plane stress and plane strain problems, Dundurs' parameters (α, β) fully control the solution and results [21]. Under fixed (α, β), therefore, the ISSFs are always the same for plane problems. However, since the cylindrical butt joint is axi-symmetric, (α, β) cannot totally control the ISSFs. Fig.8 shows an example when (α, β) = (0.8, 0.3). Fig. 8(a) and Fig. 8(b) show the possible material combinations under (α, β) = (0.8, 0.3). Here, ν_2 and E_2/E_1 are calculated by varying ν_1 from 0 to 0.5. It can be seen that ν_2 changes from 0.183 to 0.250, and E_2/E_1 changes from 0.107 to 0.139. Fig. 8(c) shows $K_\sigma^C/K_\sigma^P = [\sigma_{z0,FEM}^C - \tilde{\sigma}_{z0,FEM}^C]/\sigma_{y0,FEM}^P$ and $\sigma_{z0,FEM}^C/\sigma_{y0,FEM}^P$ calculated by varying ν_1 from 0 to 0.5. It is seen that K_σ^C/K_σ^P changes from 0.998 to 1.081, and $\sigma_{z0,FEM}^C/\sigma_{y0,FEM}^P$ changes from 0.998 to 1.032. Different from plane problems, K_σ^C/K_σ^P and $\sigma_{z0,FEM}^C/\sigma_{y0,FEM}^P$ are not constants under fixed (α, β). Therefore, in this study the maximum and minimum values will be focused to evaluate the strength of cylindrical butt joint.

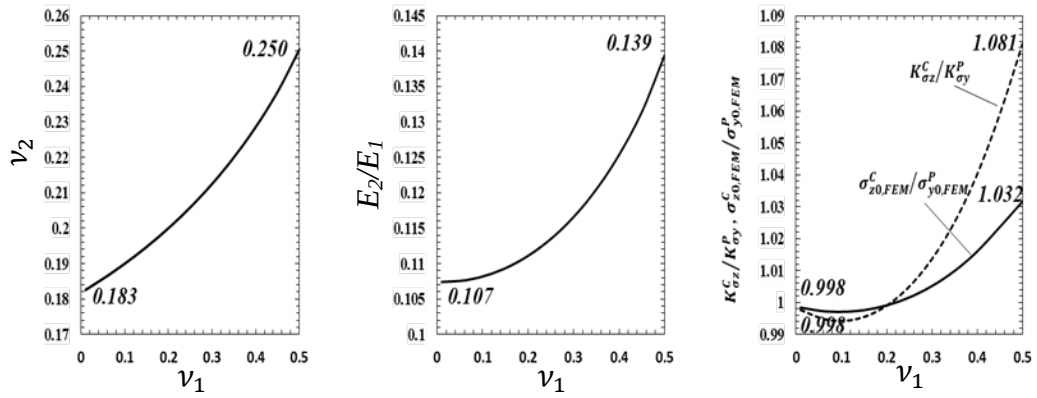

(a) (b) (c)

Fig. 8 (a) ν_2, (b) E_2/E_1, (c) K_σ^C/K_σ^P and $\sigma_{z0,FEM}^C/\sigma_{y0,FEM}^P$ values depending on ν_1 under fixed (α, β) = (0.8, 0.3)

For several material combinations, Table 9 shows normalized ISSF F_σ^C defined in Equation (23). And Fig.9 shows F_σ^C vs. *h*/*W* relation.

$$\text{Normarized ISSF } F_\sigma^C = K_\sigma^C/\sigma W^{1-\lambda}. \quad (23)$$

As shown in Fig.9 when adhesive thickness h is large, the normalized ISSF F_σ^C always becomes constant. In Table 9, the normalized ISSF F_σ^C has the same value in the range $h/W \geq 1$ since the thickness effect can be negligible.

Table 10 shows normalized ISSF F_σ^{C*} values defined in Equation (24). And Fig.10 shows F_σ^{C*} vs. h/W relation.

$$\text{Normalized ISSF } F_\sigma^{C*} = K_\sigma^P/\sigma h^{1-\lambda}. \quad (24)$$

It is seen that when the bondline thickness is small, the F_σ^{C*} value always becomes constant. From Fig.9 and Fig.10, it is found that $F_\sigma^{C*} = K_\sigma^C/\sigma h^{1-\lambda}$ is suitable for evaluating the adhesive strength when the bondline thickness is small, because F_σ^{C*} is more insensitive to small h/W than $F_\sigma^C = K_\sigma^C/\sigma W^{1-\lambda}$. As shown in Table 10, the normalized ISSF F_σ^{C*} has almost the same value in the range $h/W \leq 0.01$ within 0.3% deviation and in the range $h/W \leq 0.1$ within 4% deviation since the width effect is smaller.

Table 9 F_σ^C and $F_\sigma^C/F_\sigma^C|_{h/W\to\infty}$ of cylindrical butt joint by varying the bondline thickness

F_σ^C				
Mat / *h/W*	E_1=1000 ν_1=0.23 E_2=535.963 ν_2=0.239	E_1=1000 ν_1=0.23 E_2=339.392 ν_2=0.189	E_1=1000 ν_1=0.23 E_2=413.754 ν_2=0.293	E_1=1000 ν_1=0.23 E_2=312.891 ν_2=0.333
0.001	0.722	0.623	0.478	0.302
0.002	0.734	0.642	0.498	0.324
0.005	0.750	0.667	0.526	0.357
0.01	0.763	0.688	0.549	0.384
0.05	0.798	0.743	0.610	0.459
0.1	0.819	0.774	0.645	0.504
0.5	0.890	0.860	0.762	0.650
1	0.901	0.871	0.779	0.669
10	0.901	0.871	0.779	0.669
→∞	0.901	0.871	0.779	0.669
$F_\sigma^C/F_\sigma^C\|_{h/W\to\infty}$				
Mat / *h/W*	E_1=1000 ν_1=0.23 E_2=535.963 ν_2=0.239	E_1=1000 ν_1=0.23 E_2=339.392 ν_2=0.189	E_1=1000 ν_1=0.23 E_2=413.754 ν_2=0.293	E_1=1000 ν_1=0.23 E_2=312.891 ν_2=0.333
0.001	0.801	0.715	0.614	0.451
0.002	0.815	0.737	0.639	0.484

0.005	0.832	0.766	0.675	0.534
0.01	0.847	0.790	0.705	0.574
0.05	0.886	0.853	0.783	0.686
0.1	0.909	0.889	0.828	0.753
0.5	0.988	0.987	0.978	0.972
1	1.000	1.000	1.000	1.000
10	1.000	1.000	1.000	1.000
→∞	1.000	1.000	1.000	1.000

Table 10 F_σ^{C*} and $F_\sigma^{C*}/\,F_\sigma^{C*}|_{h/W\to 0}$ of cylindrical butt joint with varying the bondline thickness

F_σ^C				
Mat \ *h/W*	E_1=1000 ν_1=0.23 E_2=535.963 ν_2=0.239	E_1=1000 ν_1=0.23 E_2=339.392 ν_2=0.189	E_1=1000 ν_1=0.23 E_2=413.754 ν_2=0.293	E_1=1000 ν_1=0.23 E_2=312.891 ν_2=0.333
→0	0.851	0.833	0.722	0.616
0.001	0.851	0.833	0.722	0.616
0.002	0.851	0.833	0.722	0.616
0.005	0.851	0.834	0.722	0.617
0.01	0.852	0.835	0.723	0.618
0.05	0.857	0.843	0.729	0.626
0.1	0.866	0.852	0.741	0.639
0.5	0.905	0.886	0.794	0.699
1	0.901	0.871	0.779	0.669
10	0.853	0.790	0.678	0.527
$F_\sigma^{C*}/\,F_\sigma^{C*}\|_{h/W\to 0}$				
Mat \ *h/W*	E_1=1000 ν_1=0.23 E_2=535.963 ν_2=0.239	E_1=1000 ν_1=0.23 E_2=339.392 ν_2=0.189	E_1=1000 ν_1=0.23 E_2=413.754 ν_2=0.293	E_1=1000 ν_1=0.23 E_2=312.891 ν_2=0.333
→0	1.000	1.000	1.000	1.000
0.001	1.000	1.000	1.000	1.000
0.002	1.000	1.000	1.000	1.000
0.005	1.000	1.001	1.000	1.002
0.01	1.001	1.002	1.001	1.003
0.05	1.007	1.012	1.010	1.016
0.1	1.018	1.023	1.026	1.037
0.5	1.063	1.064	1.100	1.135
1	1.059	1.046	1.079	1.086
10	1.002	0.948	0.939	0.856

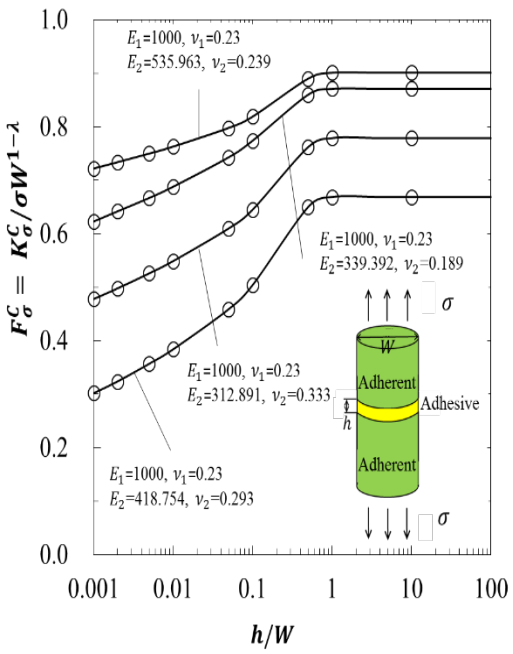

Fig.9. F_σ^C is constant when $h/W \geq 1.0$

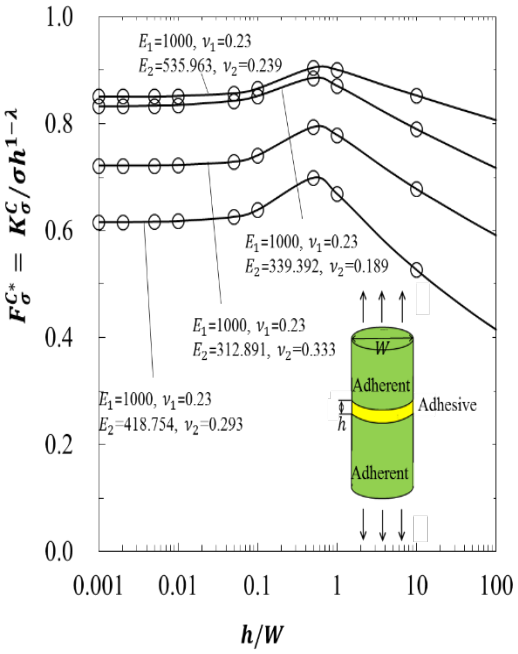

Fig.10. F_σ^{C*} is constant when $h/W \leq 0.01$

Fig. 11 and Fig. 12 show the maximum values of K_σ^C/K_σ^P and the $\sigma_{z0,FEM}^C/\sigma_{y0,FEM}^P$ by varying α from -0.2 to 1.0 when β = 0.2 and β = 0.3. Those values were calculated in a similar way as shown in Fig.8. For the bad pair $\alpha(\alpha - 2\beta) > 0$, the solid line indicates the ISSF ratio K_σ^C/K_σ^P and the broken line indicates the stress ratio $\sigma_{z0,FEM}^C/\sigma_{y0,FEM}^P$. For $\alpha(\alpha - 2\beta) > 0$, the singular stress appears at the interface end, and therefore K_σ^C/K_σ^P may be useful for evaluating the debonding strength [7-9, 12, 20]. For the good pair $\alpha(\alpha - 2\beta) < 0$, the solid line indicates the stress ratio $\left(\sigma_{z0,FEM}^C/\sigma_{y0,FEM}^P\right)_{\max}$. In this case, the singular stress does not appear at the interface end.

It is found that the ISSF ratio $(K_\sigma^C)_{\max}/K_\sigma^P \to \infty$ as $\alpha \to 2\beta$. However, it should be noted that the singular stress field disappears since the singular index $\lambda \to 1$ as $\alpha \to 2\beta$. Therefore, the stress ratio $\left(\sigma_{z0,FEM}^C/\sigma_{y0,FEM}^P\right)_{\max}$ may be useful than the ISSF ratio K_σ^C/K_σ^P around $\alpha = 2\beta$.

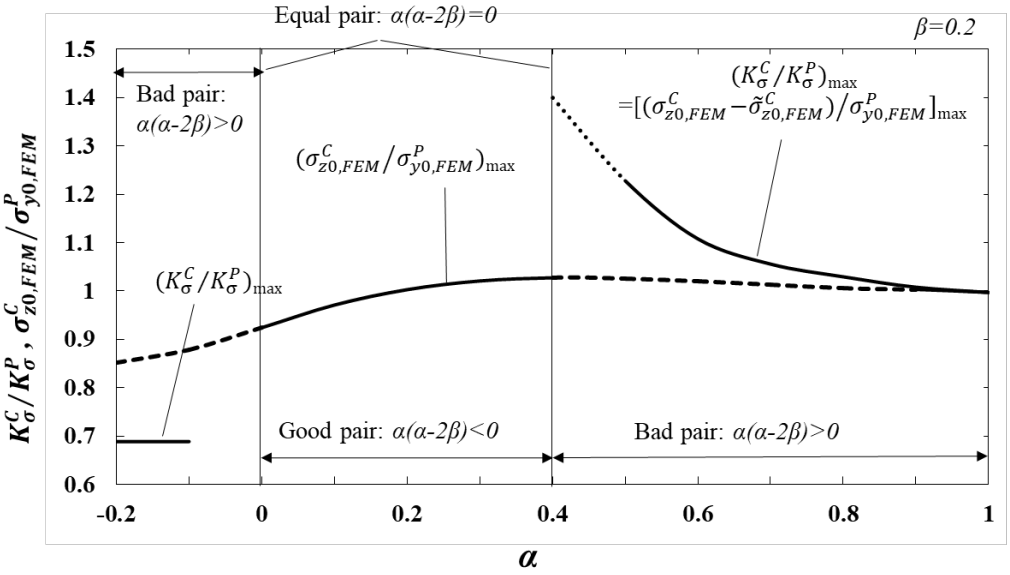

Fig. 11 Maximum values of K_σ^C/K_σ^P and $\sigma_{z0,FEM}^C/\sigma_{y0,FEM}^P$ when β = 0.2

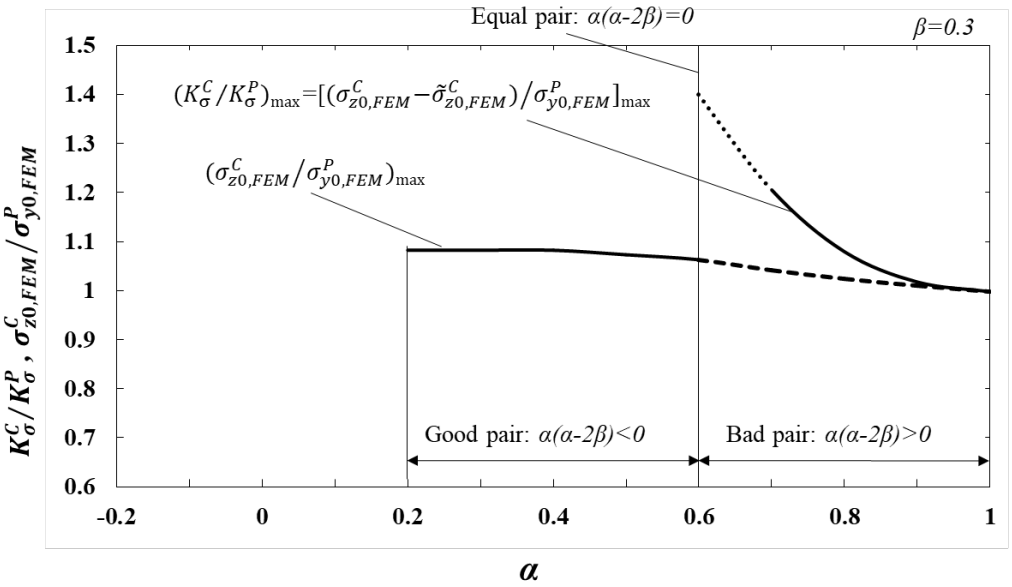

Fig. 12 Maximum values of K_σ^C/K_σ^P and $\sigma_{z0,FEM}^C/\sigma_{y0,FEM}^P$ when β = 0.3

Fig. 13 and Fig. 14 and Tables 11 and 12 show the maximum and minimum values of K_σ^C/K_σ^P and $\sigma_{z0,FEM}^C/\sigma_{y0,FEM}^P$ calculated by varying (α, β). As mentioned above, K_σ^C/K_σ^P is useful for predicting the debonding strength for bad pairs $\alpha(\alpha-2\beta)>0$, this is because the stress singularity occurs at the interface end when $\alpha(\alpha-2\beta)>0$. On the other hand, $\sigma_{z0,FEM}^C/\sigma_{y0,FEM}^P$ may be useful for predicting the debonding strength for good pairs $\alpha(\alpha-2\beta)\leq 0$. However, when $\alpha \cong$

2β, it is not known whether K_σ^C/K_σ^P or $\sigma_{z0,FEM}^C/\sigma_{y0,FEM}^P$ is suitable for predicting the strength because $(K_\sigma^C)_{\max}/K_\sigma^P$ goes to infinity when $\alpha \to 2\beta$. Figures 13 and 14 and Tables 11 and 12 are useful for $h/W \leq 0.01$ in Fig.1(c). Since the solution for $h/W \geq 1.0$ in Fig.1(c) was shown in the Appendix B, the accurate results can be obtained by the interpolation also in the range for $0.01 \leq h/W \leq 1.0$.

Fig. 15 shows the variations of the parameters in the α-β space for the materials combinations among metal, ceramics, resin, and glass [29]. Although $(K_\sigma^C)_{\max}/K_\sigma^P$ in Fig. 13 goes to infinity around the equal pair condition, $(K_\sigma^C)_{\max}/K_\sigma^P$ is less than 1.5 for most of the bad pair region $\alpha\,(\alpha - 2k\beta) \geq 0$, $k = 1.0 + 0.61(\beta^2 - 0.25)$ as indicated in Fig. 15.

$$\frac{(K_\sigma^C)_{\max}}{K_\sigma^P} \leq 1.5 \quad \text{when} \quad \alpha\,(\alpha - 2k\beta) \geq 0, \qquad k = 1.0 - 0.61(\beta^2 - 0.25) \tag{23}$$

In the previous studies [24], the authors obtained $k = 1.35 - 0.7|\beta|$ for the bonded cylinder and $k = 1.3 - 0.6|\beta|$ for the bonded pipe with the infinite inner radius. As shown in Fig. 15, the butt joint ISSF ratio satisfies less than 1.5 in the wide range of the bonded cylinder and the bonded pipe. This is because the butt joint has the small 3D effect on the ISSF in comparison with the bonded cylinder and the bonded pipe.

Fig. 15 also shows that almost all $(\alpha,\ \beta)$ of engineering materials are distributed in $0 \leq |\beta| \leq 0.3$ [24], therefore, the stress ratio $\sigma_{z0,FEM}^C/\sigma_{y0,FEM}^P$ can be discussed in this range. It should be noted that the stress ratio $\left(\sigma_{z0,FEM}^C/\sigma_{y0,FEM}^P\right)_{\max}$ is always finite in this range. Comparing Fig. 13 with Fig. 14, it is found that the value of $\sigma_{z0,FEM}^C/\sigma_{y0,FEM}^P$ varies depending on $(\alpha,\ \beta)$ but the value of $\left(\sigma_{z0,FEM}^C/\sigma_{y0,FEM}^P\right)_{\max}$ is in the small range for most of good pairs satisfying $\alpha\,(\alpha - 2\beta) < 0$ and $0 \leq |\beta| \leq 0.3$. Also, the difference between $\left(\sigma_{z0,FEM}^C/\sigma_{y0,FEM}^P\right)_{\max}$ and $\left(\sigma_{z0,FEM}^C/\sigma_{y0,FEM}^P\right)_{\min}$ is small in this region. The value range and the maximum and minimum value difference can be expressed in Eq. (24).

$$0.971 \le \left(\frac{\sigma_{z0,FEM}^{C}}{\sigma_{y0,FEM}^{P}}\right)_{\max} \le 1.143\,, \quad \frac{\left(\frac{\sigma_{z0,FEM}^{C}}{\sigma_{y0,FEM}^{P}}\right)_{\max} - \left(\frac{\sigma_{z0,FEM}^{C}}{\sigma_{y0,FEM}^{P}}\right)_{\min}}{\left(\frac{\sigma_{z0,FEM}^{C}}{\sigma_{y0,FEM}^{P}}\right)_{\max} + \left(\frac{\sigma_{z0,FEM}^{C}}{\sigma_{y0,FEM}^{P}}\right)_{\min}} \le 0.1\,, \tag{24}$$

when $0 \le |\beta| \le 0.3$ and $\alpha\,(\alpha - 2\beta) < 0$

The difference between $\left(\sigma_{z0,FEM}^{C}/\sigma_{y0,FEM}^{P}\right)_{\max}$ and $\left(\sigma_{z0,FEM}^{C}/\sigma_{y0,FEM}^{P}\right)_{\min}$ is less than 10% in Eq. (24), and therefore, Dundurs' parameters can almost control the results and be useful for axisymmetric bonded structures. For two-dimensional problems, Dundurs' parameters are most useful since they control the results completely (no difference).

Since $(K_{\sigma}^{C})_{\max}/K_{\sigma}^{P}$ goes to infinity when $\alpha \to 2\beta$, it is not clear whether $K_{\sigma}^{C}/K_{\sigma}^{P}$ or $\sigma_{z0,FEM}^{C}/\sigma_{y0,FEM}^{P}$ is suitable for predicting the strength at present.

Useful parameter is unknown near the equal pair
$\alpha\,(\alpha - 2k\beta) < 0, k = 1.0 - 0.61(\beta^2 - 0.25)$ and $\alpha\,(\alpha - 2\beta) \ge 0$ in Fig. 15 (25)

Table 11 Maximum and minimum values of $K_{\sigma}^{C}/K_{\sigma}^{P}$ which is useful for $h/W \le 0.01$ in Fig.1(c)

α \ β	-0.4	-0.3	-0.2	-0.1	0	0.1	0.2	0.3	0.4
-1	1.220 0.977	1.102 0.945	0.951 0.838	0.696 0.697	0.615 0.636				
-0.9	1.294 0.986	1.141 0.949	0.991 0.845	0.738 0.703	0.652 0.646				
-0.8		1.187 0.956	1.044 0.855	0.819 0.722	0.720 0.670				
-0.7		1.260 0.978	1.121 0.875	0.906 0.748	0.779 0.709				
-0.6			1.258 0.889	0.988 0.771	0.829 0.737	0.650 0.684			
-0.5			1.364 0.902	1.043 0.791	0.887 0.758	0.687 0.704			
-0.4				1.108 0.811	0.919 0.776	0.708 0.721			
-0.3				1.153 0.834	0.938 0.796	0.736 0.736			
-0.2					0.952 0.825	0.779 0.749	0.688 0.658		
-0.1					0.962 0.861	0.795 0.763	0.698 0.683		
0			0.987 0.961	0.989 0.895		0.803 0.775	0.710 0.698		
0.1			0.987	0.990	0.991				

			0.972	0.914	0.924				
0.2			0.987 0.981	0.991 0.938	0.992 0.942				
0.3				0.992 0.951	0.993 0.954	1.153 0.971			
0.4				0.992 0.960	0.994 0.965	1.052 0.972			
0.5				0.993 0.966	0.994 0.973	1.022 0.977	1.228 0.988		
0.6				0.994 0.970	0.995 0.980	1.010 0.982	1.108 0.987		
0.7					0.994 0.985	1.003 0.986	1.056 0.989	1.205 0.994	
0.8					0.995 0.987	1.000 0.990	1.029 0.992	1.079 0.995	
0.9					0.996 0.989	1.000 0.995	1.008 0.996	1.018 0.997	1.091 0.999
1					0.996 0.991	0.996 0.996	0.997 0.997	0.998 0.998	1.000 1.000

Upper: maximum value, lower: minimum value

Table 12 Maximum and minimum values of $\sigma^{C}_{z0,FEM}/\sigma^{P}_{y0,FEM}$ which is useful for $h/W \le 0.01$ in Fig.1(c)

Table 12 Maximum and minimum values of $\sigma^{C}_{z0,FEM}/\sigma^{P}_{y0,FEM}$ which is useful for $h/W \le 0.01$ in Fig.1(c)

α \ β	-0.4	-0.3	-0.2	-0.1	0	0.1	0.2	0.3	0.4
-1	1.001 1.001	0.966 0.966	0.922 0.922	0.856 0.856	0.815 0.815				
-0.9	1.032 1.016	0.988 0.974	0.937 0.931	0.879 0.874	0.832 0.830				
-0.8	1.085 1.035	1.011 0.983	0.968 0.942	0.896 0.891	0.844 0.841				
-0.7	1.136 1.047	1.052 0.993	0.996 0.956	0.934 0.911	0.861 0.853				
-0.6		1.103 1.001	1.037 0.969	0.992 0.925	0.890 0.864	0.826 0.826			
-0.5		1.131 1.013	1.075 0.987	1.025 0.947	0.921 0.876	0.831 0.831			
-0.4		1.143 1.021	1.095 1.000	1.044 0.963	0.952 0.889	0.846 0.846			
-0.3		1.134 1.024	1.101 1.004	1.044 0.982	0.973 0.909	0.866 0.866			
-0.2		1.121 1.024	1.087 1.006	1.043 1.000	0.987 0.949	0.901 0.901	0.861 0.861		
-0.1			1.065 1.005	1.039 1.001	0.995 0.983	0.939 0.929	0.879 0.879		
0			1.045 1.003	1.032 1.001	1.000 1.000	0.966 0.965	0.924 0.924		
0.1			1.029 1.003	1.020 1.000	1.004 1.000	0.992 0.986	0.971 0.971		

0.2			1.003 1.003	1.003 0.998	1.002 0.999	1.000 0.998	1.003 0.989	1.082 1.010	
0.3				1.000 0.996	0.999 0.997	1.004 0.999	1.021 0.996	1.082 1.009	
0.4				0.996 0.995	0.997 0.994	1.006 0.996	1.027 0.997	1.082 1.008	
0.5				0.996 0.994	0.996 0.992	1.005 0.994	1.026 0.998	1.073 1.006	
0.6				0.995 0.993	0.996 0.991	1.004 0.992	1.020 0.996	1.063 1.000	
0.7					0.995 0.991	1.001 0.992	1.013 0.994	1.042 0.998	1.085 1.001
0.8					0.995 0.991	1.000 0.993	1.006 0.995	1.024 0.997	1.054 1.000
0.9					0.995 0.991	1.000 0.996	1.003 0.997	1.010 0.998	1.025 1.000
1					0.996 0.991	0.996 0.996	0.997 0.997	0.998 0.998	1.000 1.000

Upper: maximum value, lower: minimum value

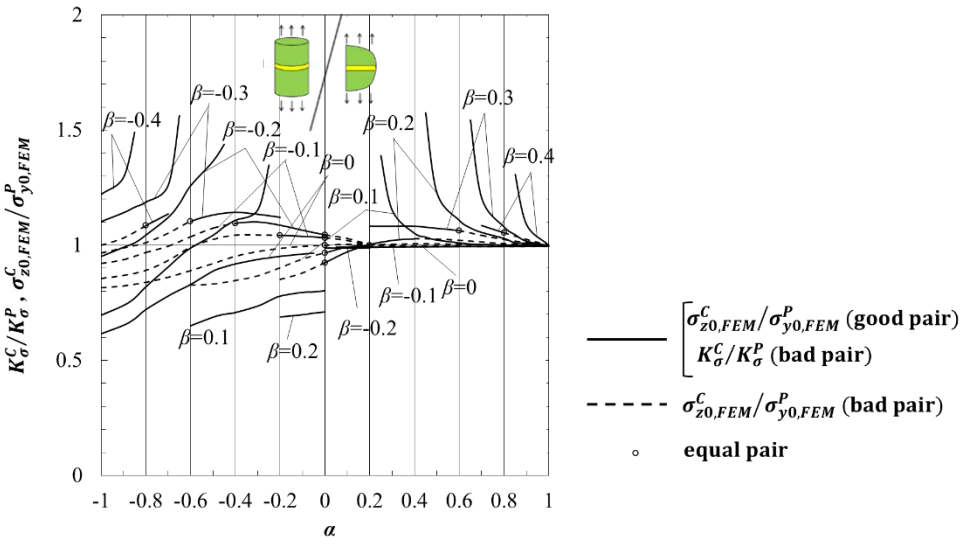

Fig. 13 Maximum value of K_σ^C/K_σ^P and $\sigma_{z0,FEM}^C/\sigma_{y0,FEM}^P$ which is useful for $h/W \leq 0.01$ in Fig.1(c)

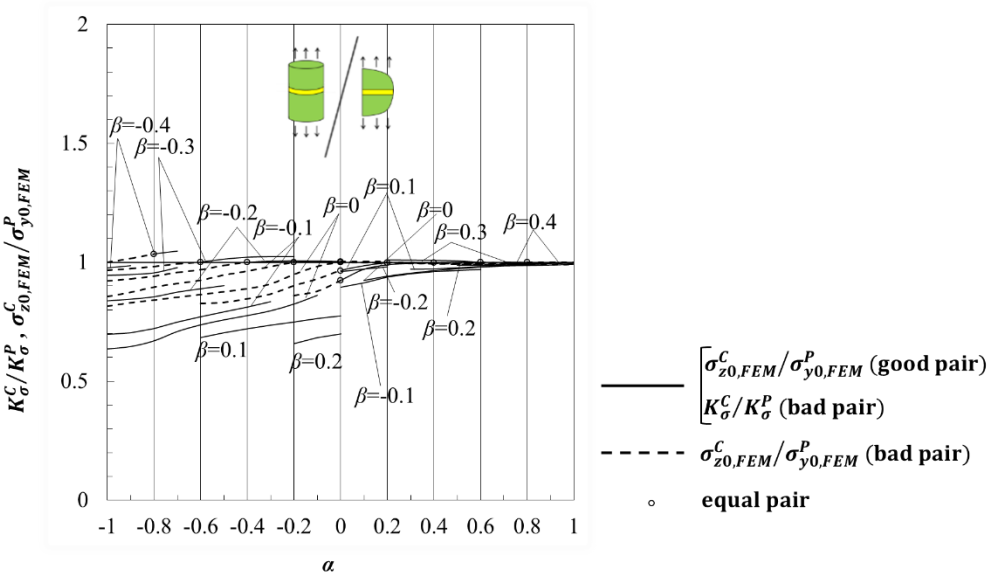

Fig. 14 Minimum value of K_σ^C/K_σ^P and $\sigma_{z0,FEM}^C/\sigma_{y0,FEM}^P$ which is useful for $h/W \leq 0.01$ in Fig.1(c)

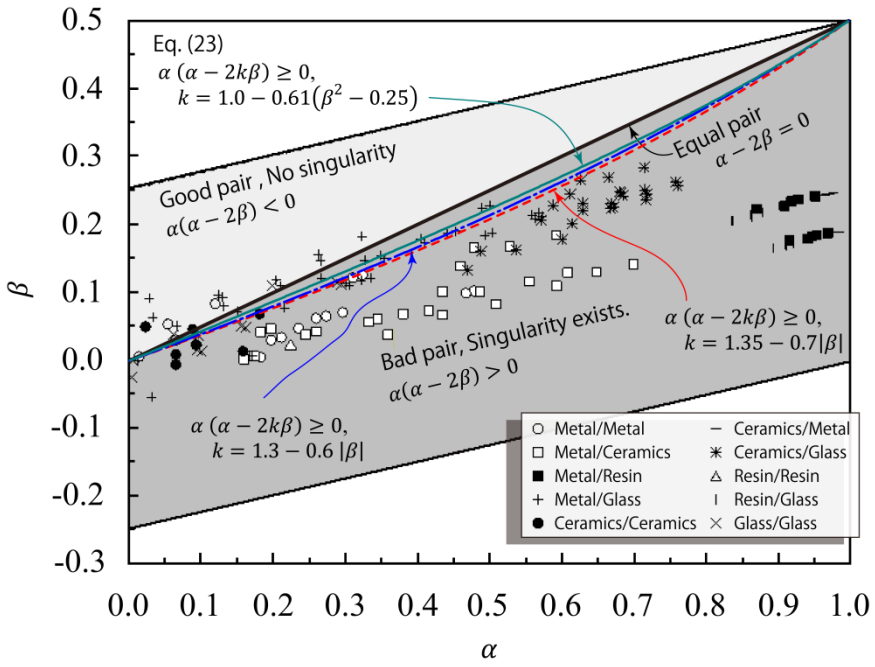

Fig. 15 Dundurs' parameters for the several engineering materials and the range of $(\alpha,\ \beta)$ satisfies ISSF ratio < 1.5[24]

5. Experimental evaluation of debonding strength of cylindrical butt joint and plate butt joint

The debonding strength of the cylindrical butt joints was studied experimentally by several researchers [30]. Fig. 16 shows the schematic

illustration of the specimens. In this experiment of Naito et al [30], the adherent is aluminum alloy 5052-H34 (Young's modulus E_1 = 69.6GPa, Poisson's ratio v_1 = 0.33) and the adhesive is polyimide (E_2 = 3.77GPa, v_2 = 0.342). Table 13(a), (b) show Dundurs' parameters (α, β) and singular index λ. The length of the adherent l is 38.1 mm and the adhesive thickness t is varied from 0.2mm to 0.6mm.

Fig. 17(a) shows the tensile strength σ_c which increases with increasing the adhesive thickness. In the experiment, the fracture was initiated at the axisymmetric interface end between the adhesive and the adherent. Fig. 17(b) shows the dimensionless of ISSFs for the cylindrical butt joint $F_\sigma^C = K_\sigma^C / (\sigma_z^\infty W^{1-\lambda})$ and $F_\sigma^{C*} = K_\sigma^C / (\sigma_z^\infty h^{1-\lambda})$ obtained by the method shown in Section 4. In Fig.17(b) F_σ^C and F_σ^{C*} increase with increasing the adhesive thickness. However, F_σ^{C*} is insensitive of *h/W* and almost constant within 2%. It is seen that F_σ^{C*} can be used conveniently to evaluate the adhesive strength. Fig. 17(c) shows the critical ISSF at $\sigma_z^\infty = \sigma_c$, $K_{\sigma c} = K_\sigma^C \,|_{\sigma_z^\infty = \sigma_c}$. The $K_{\sigma c}$ values are almost constant independent of the adhesive thickness. It can be confirmed that the ISSF is useful for evaluating the debonding strength.

Similarly, the debonding strength of the plate butt joints [15] was considered again by using the present results. Fig. 18 (a), (d) shows the tensile strength σ_c. σ_c increases with increasing the adhesive thickness. In Suzuki's experiment [15], it was observed that the fracture is initiated from the interface end between the adhesive and the adherent. Fig. 18 (b),(e) shows the ISSFs for the cylindrical butt joint $F_\sigma^P = K_\sigma^P / (\sigma_z^\infty W^{1-\lambda})$ and $F_\sigma^{P*} = K_\sigma^P / (\sigma_z^\infty h^{1-\lambda})$ obtained by the method shown in Section 4. In Fig.18 (c),(f) F_σ^P and F_σ^{P*} increase with increasing the bondline thickness. However, F_σ^{P*} is also insensitive of *h/W* and almost constant with 2%. It is seen that F_σ^{P*} can be used conveniently to evaluate the adhesive strength. Fig. 18 (c),(f) shows the critical ISSF at $\sigma_z^\infty = \sigma_c$, $K_{\sigma c} = K_\sigma^P \,|_{\sigma_z^\infty = \sigma_c}$. The $K_{\sigma c}$ values are almost constant independent of the bondline thickness. It can be confirmed that the ISSF is useful for evaluating the debonding strength.

Table 13 Results of cylindrical butt joint in Fig.16 [30]

(a) Dundurs' parameters (α, β) and order of singular index λ in cylindrical butt joint(aluminum/polyimide)

Materials	Adherend		Adhesive		Dundurs' parameter		Singular index
	E_1 [GPa]	ν_1	E_2 [GPa]	ν_2	α	β	λ
Aluminum/Polyimide	69.9	0.33	3.77	0.342	0.8963	0.2145	0.7398

(b)Tensile strength σ_c, F_σ^C, F_σ^{C*}, $K_{\sigma c}$ for plate butt joint

h	h/W	S35C/Epoxy resin A				S35C/Epoxy resin B			
		σ_c [MPa]	F_σ^C	F_σ^{C*}	$K_{\sigma c}$	σ_c [MPa]	F_σ^C	F_σ^{C*}	$K_{\sigma c}$
0.05	0.00394	57.2	0.0671	0.384	0.970	76.8	0.0620	0.377	1.15
0.1	0.00787	53.3	0.0831	0.382	1.120	71.4	0.0778	0.377	1.34
0.3	0.0236	32.5	0.119	0.387	0.978	49.7	0.112	0.380	1.34
0.6	0.0472	25.9	0.150	0.392	0.981	41.2	0.142	0.384	1.41
1.0	0.0787	22.6	0.178	0.396	1.020	25.3	0.171	0.392	1.04

Table 14 Results of plate butt joint [15]

(a)Dundurs' parameters (α, β) and order of singular index λ

Materials	Adherend		Adhesive		Dundurs' parameter		Singular index
	E_1 [GPa]	ν_1	E_2 [GPa]	ν_2	α	β	λ
S35C/Epoxy resin A	210	0.30	3.14	0.37	0.969	0.199	0.685
S35C/Epoxy resin B	210	0.30	2.16	0.38	0.978	0.188	0.674

(b) Tensile strength σ_c, F_σ^C, F_σ^{C*}, $K_{\sigma c}$ for the specimen in Fig.16 with *l*=38.1mm, *t*=0.2~0.6mm, *W*=12.7mm

h	h/W	σ_c [MPa]	F_σ^C	F_σ^{C*}	$K_{\sigma c}$
0.02	0.0157	22.5	0.154	0.453	1.109
0.03	0.0236	20.9	0.172	0.456	1.155
0.04	0.0315	18.6	0.186	0.458	1.111
0.05	0.0394	17.5	0.198	0.460	1.114
0.06	0.0472	15.7	0.209	0.462	1.052

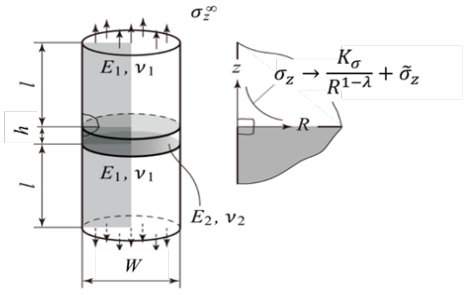

Fig. 16 Schematic illustration of cylindrical butt joint

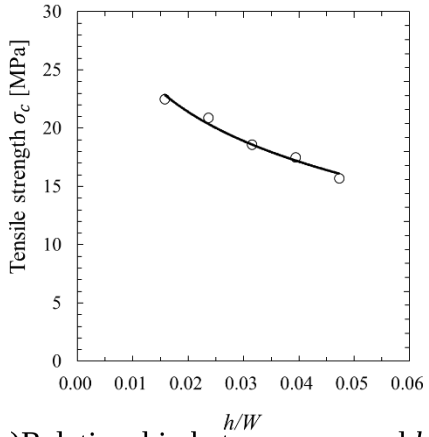

(a)Relationship between σ_c and h/W

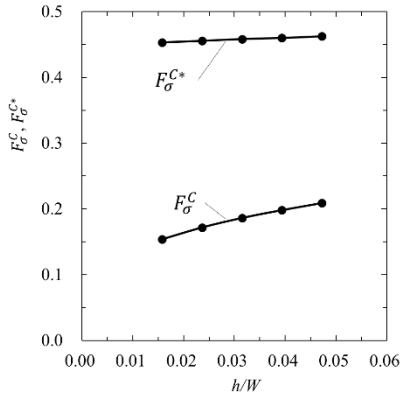

(b)Relationship between F_σ^C, F_σ^{C*} and h/W

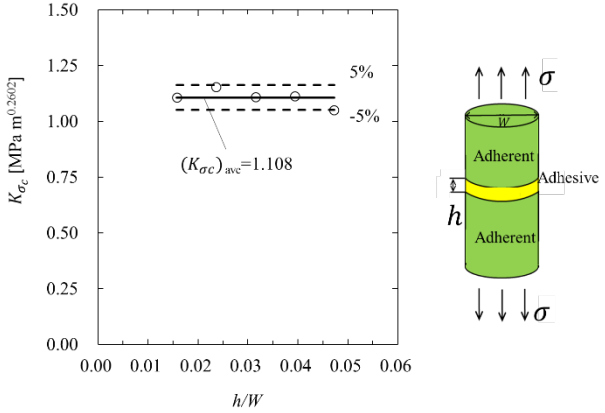

(c) Critical value of ISSF, $K_{\sigma c}$

Fig. 17 Results of cylindrical butt joint in Fig.15[17]

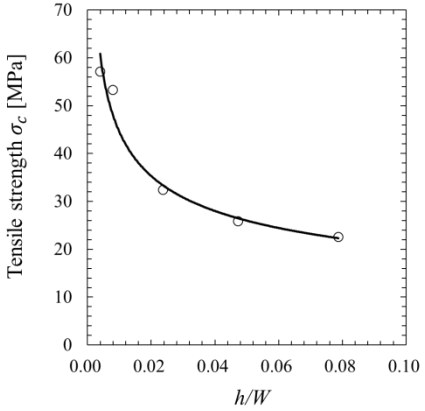

(a)Relationship between σ_c and h/W

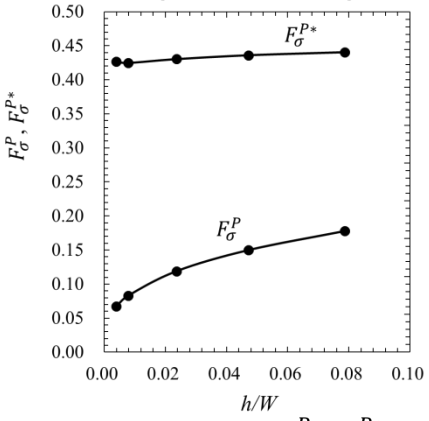

(b)Relationship between F_σ^P, F_σ^{P*} and h/W

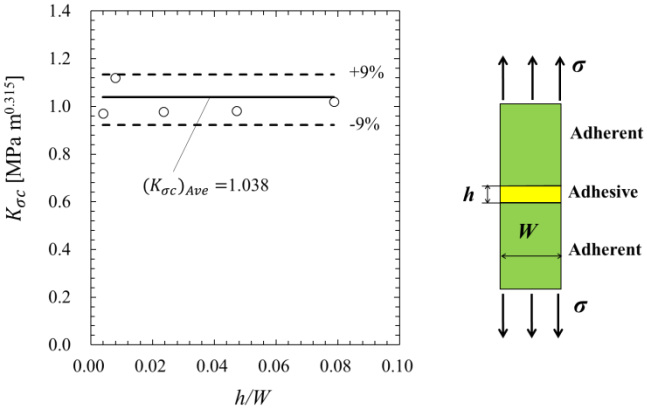

(c) Critical value of ISSF, $K_{\sigma c}$

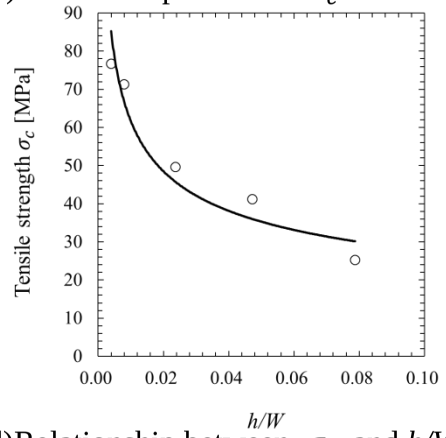

(d)Relationship between σ_c and h/W

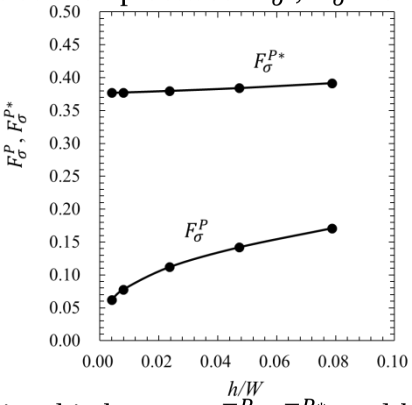

(e) Relationship between F_σ^P, F_σ^{P*} and h/W

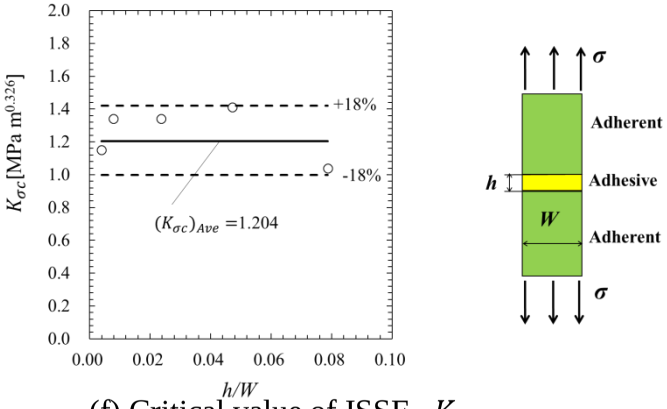

(f) Critical value of ISSF, $K_{\sigma c}$

Fig. 18 Results of plate butt joint

6. Conclusions

In this study, the ISSF variations were clarified over the entire thickness range of plate and cylinder butt joints. An effective mesh-independent technique was applied to obtaining the ISSFs under arbitrary material combinations. A reference solution was used to eliminate FEM error since the solutions are available for simple bonded plate solved by the body force method. Then, the following conclusions can be summarized.

(1) For the plate butt joints, the ISSF $F_\sigma^{P*} = K_\sigma^P/\sigma h^{1-\lambda}$ normalized by the bondline thickness h becomes constant with decreasing the bondline thickness when $h/W \leq 0.01$. In this case, the adhesive joint can be regarded as a bonded semi-infinite plate. If the adhesive layer is thin, F_σ^{P*} is more suitable because the variation is smaller than the variation of $F_\sigma^P = K_\sigma^P/\sigma W^{1-\lambda}$. To improve the interface strength, thin adhesive layers are desirable. For a certain value β, it is found that F_σ^{P*} decreases with increasing α. Since the solution for $h/W \geq 1.0$ in Fig.1(a) was shown in the Appendix A, the accurate results can be obtained by the interpolation also in the range for $0.01 \leq h/W \leq 1.0$.

(2) For the cylindrical butt joint, the circumferential strain at the interface end, ε_{r0}^C, is not influenced by the stress singularity because ε_{r0}^C is obtained from the radial displacement u_{r0}^C and the cylinder radius. It was found that the non-singular stresses caused by the ε_{r0}^C are contained in the FEM stresses at the interface end. The accurate method was therefore used for calculating the ISSF from the ratio of the stress obtained by subtracting the non-singular stress to the stress of the semi-infinite butt joint adopted as the reference solution. The stress-free boundary condition causes the nonsingular stresses $\tilde{\sigma}_{r0,FEM}^C = \tilde{\tau}_{rz0,FEM}^C = 0$. The ISSF can be calculated easily without subtraction process of the non-singular stresses when the radial stress $\sigma_{r0,FEM}^C$ or the shear stress $\tau_{rz,FEM}^C$ is used.

(3) For a certain material combination, the ISSF F_σ^{C*} normalized by adhesive thickness h becomes constant with decreasing the bondline thickness when $h/W \leq 0.01$. Thin adhesive layer can be used to improve the interface strength of the cylindrical butt joint. Since the ISSFs of the cylindrical butt joint cannot be totally dominated by the Dundurs' parameter α and β, the maximum and minimum values of the K_σ^C/K_σ^P and the $\sigma_{z0,FEM}^C/\sigma_{y0,FEM}^P$ were shown in the

charts and tables for various (α,β). The value K_σ^C/K_σ^P may be useful for predicting the debonding strength under the bad pairs $\alpha(\alpha - 2\beta) > 0$. On the other side, the $\sigma_{z0,FEM}^C/\sigma_{y0,FEM}^P$ may be more important for predicting the debonding strength under the good pairs $\alpha(\alpha - 2\beta) \leq 0$. Since the solution for $h/W \geq 1.0$ in Fig.1(c) was shown in the Appendix B, the accurate results can be obtained by the interpolation also in the range for $0.01 \leq h/W \leq 1.0$.

Appendix A: ISSF for the bonded plate

Figure A1 shows the ISSF F_σ^P for the bonded plate calculated by varying Dundurs' parameter (α,β)[14]. Then, the non-dimensional function of θ has been already clarified by Carenter and Byers[32]. The bonded plate in Fig.A1 can be regarded as a plate butt joint with a very thick adhesive layer for $h/W \geq 1.0$. The F_σ^P values are obtained by the body force method under the bad pair condition of $\alpha(\alpha - 2\beta) > 0$ [14] and obtained by FEM under the good pair condition of $\alpha(\alpha - 2\beta) < 0$ [7-9, 20]. Since the solution for thin adhesive layer $h/W \leq 0.01$ is indicated in Table 4 and Fig.7 under aribitrary material combination, the accurate results can be obtained by the interpolation also in the range for $0.01 \leq h/W \leq 1.0$.

Table A1 F_σ^P of bonded plate useful for $h/W \geq 1.0$ in Fig.1 (a)

		β								
		-0.4	-0.3	-0.2	-0.1	0.0	0.1	0.2	0.3	0.4
α	-1.00	0.540	0.446	0.395	0.357	0.332	—	—	—	—
	-0.95	0.643	0.491	0.422	0.381	0.349	—	—	—	—
	-0.90	0.726	0.534	0.456	0.412	0.381	—	—	—	—
	-0.80	1.000	0.636	0.538	0.487	0.450	—	—	—	—
	-0.70	1.855	0.800	0.626	0.558	0.486	—	—	—	—
	-0.60	3.291	1.000	0.724	0.638	0.559	0.505	—	—	—
	-0.50	—	1.264	0.842	0.722	0.635	0.551	—	—	—
	-0.40	—	1.467	1.000	0.822	0.718	0.615	—	—	—
	-0.30	—	1.609	1.118	0.913	0.796	0.697	—	—	—
	-0.20	—	1.690	1.153	1.000	0.889	0.797	0.404	—	—
	-0.10	—	—	1.103	1.037	0.955	0.890	0.767	—	—
	0.00	—	—	1.000	1.000	1.000	1.000	1.000	—	—
	0.10	—	—	0.767	0.890	0.955	1.037	1.103	—	—
	0.20	—	—	0.404	0.797	0.889	1.000	1.153	1.690	—

	0.30	—	—	—	0.697	0.796	0.913	1.118	1.609	—
	0.40	—	—	—	0.615	0.718	0.822	1.000	1.467	—
	0.50	—	—	—	0.551	0.635	0.722	0.842	1.264	—
	0.60	—	—	—	0.505	0.559	0.638	0.724	1.000	3.291
	0.70	—	—	—	—	0.486	0.558	0.626	0.800	1.855
	0.80	—	—	—	—	0.450	0.487	0.538	0.636	1.000
	0.90	—	—	—	—	0.381	0.412	0.456	0.534	0.726
	0.95	—	—	—	—	0.349	0.381	0.422	0.491	0.643
	1.00	—	—	—	—	0.332	0.357	0.395	0.446	0.540

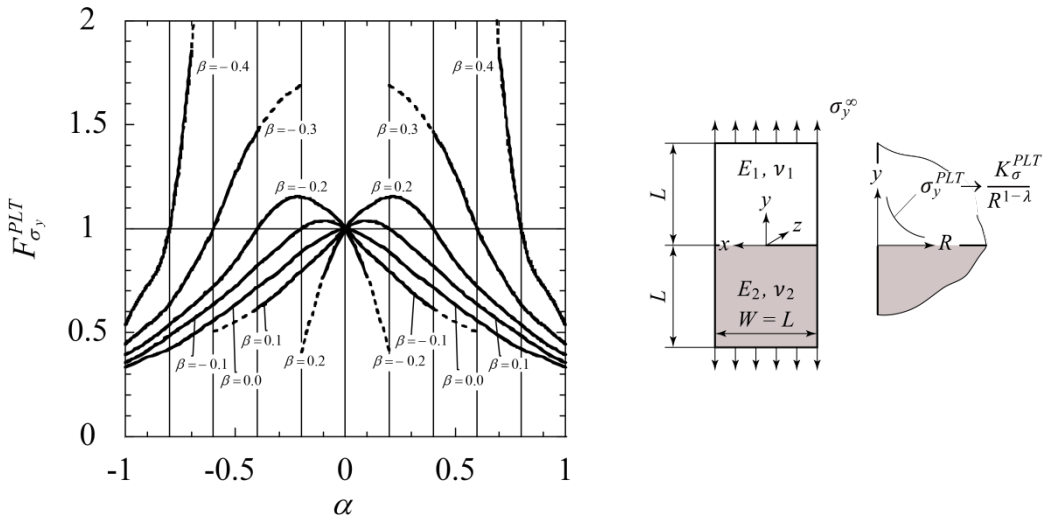

Fig. A1 ISSF for the bonded plate useful for $h/W \geq 1.0$ in Fig.1(a)

Appendix B: ISSF for the bonded cylinder in comparison with the bonded plate

In the previous study [24], the ISSF of bonded cylinder was compared with the ISSF of bonded plate under arbitrary material combination. The bonded cylinder can be regarded as a cylindrical butt joint with a very thick adhesive layer for $h/W \geq 1.0$ in Fig.1 (c). Table B1 and Figure B1 show the maximum values and the minimum values of K_σ^C/K_σ^P and $\sigma_{z0,FEM}^C/\sigma_{y0,FEM}^P$ calculated by varying(α, β). The solid lines indicate K_σ^C/K_σ^P under $\alpha(\alpha-2\beta)>0$ and $\sigma_{z0,FEM}^C/\sigma_{y0,FEM}^P$ under $\alpha(\alpha-2\beta)<0$. The dahed lines indicate $\sigma_{z0,FEM}^C/\sigma_{y0,FEM}^P$ with $\alpha(\alpha-2\beta)>0$. The circle marks indicate $\sigma_{z0,FEM}^C/\sigma_{y0,FEM}^P$ for $\alpha(\alpha-2\beta)=0$. All K_σ^C/K_σ^P values are distributed between $(K_\sigma^C)_{\max}/K_\sigma^P$ and $(K_\sigma^C)_{\min}/K_\sigma^P$. Because $(K_\sigma^C)_{\max}/K_\sigma^P$ goes to ∞ when $\alpha \to 2\beta$, the solid lines are very important for predicting the debonding

strength except for the bad pair condition near $\alpha \cong 2\beta$. Because there are only 10% differences between $(K_\sigma^C)_{\max}/K_\sigma^P$ and $(K_\sigma^C)_{\min}/K_\sigma^P$ except for the bad pair condition near $\alpha \cong 2\beta$, K_σ^C/K_σ^P and $\sigma_{z0,FEM}^C/\sigma_{y0,FEM}^P$ can be almost controlled by $(\alpha,\ \beta)$. Since the solution for thin adhesive layer $h/W \le 0.01$ is indicated in Table 11, Table 12, Fig.13 and Fig.14 under aribitrary material combination, the accurate results can be obtained by the interpolation also in the range for $0.01 \le h/W \le 1.0$.

Table B1 Maximum and minimum values of K_σ^C/K_σ^P useful for $h/W \ge 1.0$ in Fig. 1 (c)

		β										
		-0.45	0.4	0.3	-0.2	-0.1	0.0	0.1	0.2	0.3	0.4	0.45
α	-1.0	0.995	0.981	0.937	0.898	0.866	0.839					
	-0.9		1.146 0.992	0.996 0.944	0.935 0.899	0.892 0.863	0.859 0.834					
	-0.8			1.089 0.957	0.977 0.906	0.919 0.865	0.879 0.832					
	-0.7			1.321 0.976	1.032 0.918	0.948 0.870	0.899 0.833					
	-0.6				1.121 0.936	0.981 0.88	0.918 0.837	0.802				
	-0.5				1.346 0.962	1.022 0.895	0.937 0.843	0.827 0.804				
	-0.4					1.084 0.916	0.955 0.854	0.845 0.808				
	-0.3					1.234 0.944	0.972 0.87	0.856 0.814				
	-0.2						0.986 0.885	0.861 0.825	0.775			
	-0.1						0.996 0.896	0.855 0.835	0.789 0.781			
	0.0				0.791 0.789	0.866 0.820	1.000	0.866 0.820	0.791 0.789			
	0.1				0.789 0.781	0.855 0.835	0.996 0.896					
	0.2				0.775	0.861 0.825	0.986 0.885					
	0.3					0.856 0.814	0.972 0.870	1.234 0.944				
	0.4					0.845 0.808	0.955 0.854	1.084 0.916				
	0.5					0.827 0.804	0.937 0.843	1.022 0.895	1.346 0.962			
	0.6					0.802	0.918 0.837	0.981 0.88	1.121 0.936			
	0.7						0.899 0.833	0.948 0.870	1.032 0.918	1.321 0.976		
	0.8						0.879 0.832	0.919 0.865	0.977 0.906	1.089 0.957		
	0.9						0.859 0.834	0.892 0.863	0.935 0.899	0.996 0.944	1.146 0.992	
	1						0.839	0.866	0.898	0.937	0.981	0.995

Table B2 Maximum and minimum values of $\sigma^{C}_{z0,FEM}/\sigma^{P}_{y0,FEM}$ useful for $h/W \geq 1.0$ in Fig.1 (c)

		β										
		-0.45	-0.4	-0.3	-0.2	-0.1	0.0	0.1	0.2	0.3	0.4	0.45
α	-1.0	0.995	0.981	0.937	0.898	0.866	0.839					
	-0.9	1.237 1.000	1.098 0.994	0.993 0.945	0.934 0.900	0.892 0.864	0.859 0.834					
	-0.8	2.276	1.327 1.000	1.066 0.962	0.974 0.909	0.919 0.866	0.879 0.833					
	-0.7		1.862 1.564	1.165 0.986	1.020 0.925	0.946 0.875	0.899 0.835					
	-0.6		3.117	1.299 1.000	1.071 0.951	0.975 0.890	0.918 0.843					
	-0.5			1.447 1.134	1.127 0.983	1.000 0.914	0.937 0.857					
	-0.4			1.525 1.343	1.172 1.000	1.031 0.948	0.955 0.880					
	-0.3			1.444 1.358	1.184 1.036	1.050 0.984	0.972 0.914					
	-0.2			1.246	1.145 1.060	1.052 1.000	0.986 0.955					
	-0.1				1.065 1.022	1.032 1.000	0.996 0.989					
	0.0				0.978 0.948	0.997 0.981	1.000	0.997 0.981	0.978 0.948			
	0.1				0.903 0.878	0.956 0.936	0.996 0.989	1.032 1.000	1.065 1.022			
	0.2				0.844	0.920 0.896	0.986 0.955	1.052 1.000	1.145 1.060	1.246		
	0.3					0.889 0.850	0.972 0.914	1.050 0.984	1.184 1.036	1.444 1.358		
	0.4					0.863 0.826	0.955 0.880	1.031 0.948	1.172 1.000	1.525 1.343		
	0.5					0.838 0.812	0.937 0.857	1.000 0.914	1.127 0.983	1.447 1.134		
	0.6					0.808	0.918 0.843	0.975 0.890	1.071 0.951	1.299 1.000	3.117	
	0.7						0.899 0.835	0.946 0.875	1.020 0.925	1.165 0.986	1.862 1.564	
	0.8						0.879 0.833	0.919 0.866	0.974 0.909	1.066 0.962	1.327 1.000	2.276
	0.9						0.859 0.834	0.892 0.864	0.934 0.900	0.993 0.945	1.098 0.994	1.237 1.000
	1.0						0.839	0.866	0.898	0.937	0.981	0.995

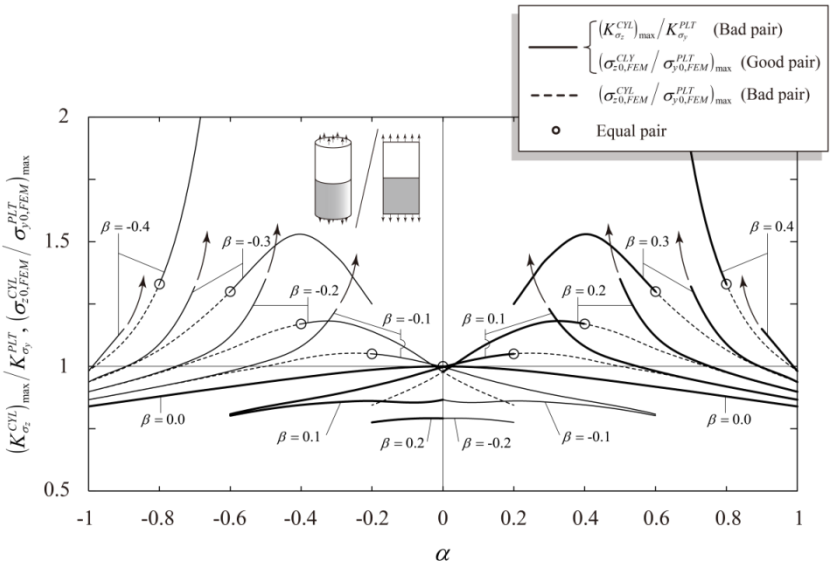

(a) Maximum values

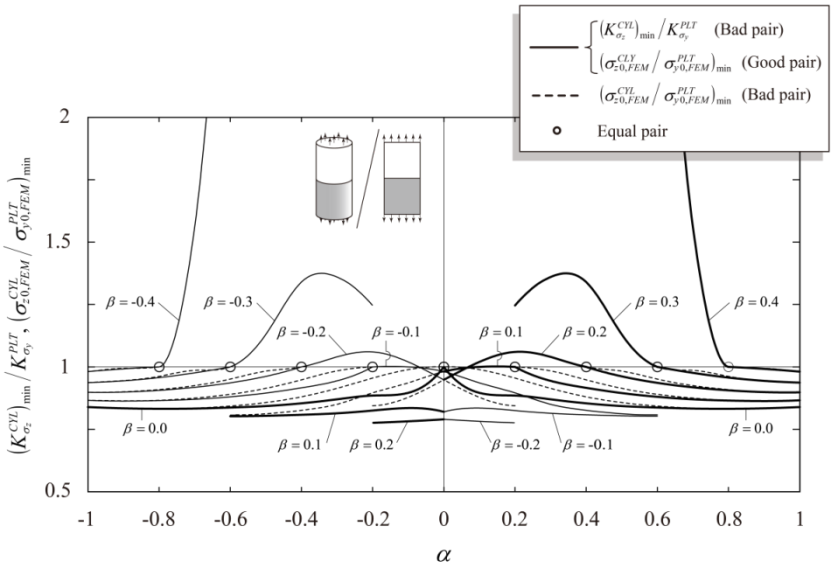

(b) Minimum values

Fig. B1 K_σ^C/K_σ^P and $\sigma_{z0,FEM}^C/\sigma_{y0,FEM}^P$ in $(\alpha,\ \beta)$ map useful for *h/W*≥1.0 in Fig.1 (c)

References

[1] Barnes, T.A., Pashby, I.R., Joining techniques for aluminium spaceframes used in automobiles: part II – adhesive bonding and mechanical fasteners. J Mater Process Technol, Vol.99, pp.72-79, 2000.

[2] Higgins, A., Adhesive bonding of aircraft structures. Int J Adhes Adhes, Vol.20, No.5, pp.367-376, 2000.

[3] Petrie, E.M., Adhesives for the assembly of aircraft structures and components: decades of performance improvement, with the new applications of the horizon. Metal Finish, Vol.106, No.2, pp.26-31, 2008.
[4] Qian Z, Akisanya, A.R., An experimental investigation of failure initiation in bonded joints. Acta Mater, Vol.46, No.14, pp.4895-4904, 1998
[5] Akisanya, A.R., Meng C.S., Initiation of fracture at the interface corner of bi-material joints. J Mech Phys Solids, Vol.51, pp.27-46, 2003.
[6] Mintzas, A, Nowell, D., Validation of an Hcr -based fracture initiation criterion for adhesively bonded joints. Eng Fract Mech, Vol.80, pp.13-27, 2012.
[7] Zhang, Y., Noda, N.A., Takaishi, K.T., Lan, X., Effect of Adhesive Thickness on the Interface of Singular Stress at the Adhesive Dissimilar Joint. Transactions of the Japan Society of Mechanical Engineers Series A , Vol. 77(774), pp. 360-372, 2011.
[8] Zhang, Y., Noda, N.A, Wu, P.Z, Duan, M.L., A Mesh-Independent Technique to Evaluate Stress Singularities in Adhesive Joints, International Journal of Adhesion & Adhesives, Vol. 57, pp. 105-117, 2015.
[9] Zhang, Y., Noda, N.A., Wu, P. and Duan, M., Corrigendum to “A mesh-independent technique to evaluate stress singularities in adhesive joints”, Vol. 60, pp. 130, 2015.
[10] Miyazaki, T., Noda, N.A., Li, R., Uchikoba, T., Sano, Y., Debonding criterion for single lap joints from the intensity of singular stress field. Transactions of The Japan Institute of Electronics Packaging, Vol.16, No.2, pp.143-151, 2013. [in Japanese].
[11] Miyazaki, T., Noda N.A., Uchikoba, T., Li, R., Sano, Y., Proposal of a convenient and accurate method for evaluation of debonding strength. Trans Soc Autom Eng Jpn, Vol.45, No.5, pp.895-901, 2014. [in Japanese].
[12] Noda, N.A., Miyazaki, T., Li, R., Uchikoba, T., Sano, Y., Takase, Y., Debonding Strength Evaluation in Terms of the Intensity of Singular Stress at the corner with and without fictitious crack, International Journal of Adhesion & Adhesives, vol. 61, pp. 46-64, 2015.
[13] Chen, D.H., Nisitani, H., Intensity of singular stress field near the interface edge point of a bonded strip. Trans. JSME 59, 2682-2686, 1993.

[14] Noda, N.A, Shirao, R., Li, J., Sugimoto, J.S., Intensity of Singular Stress at the End of a Fiber under Pull-out Force, International Journal of Solids and Structures, Vol. 44, No.13, pp.4472-4491, 2007.
[15] Suzuki, Y., Adhesive Tensile Strengths of Scarf and Butt Joints of Steel Plates, Trans. JSME, Series A, Vol.53, pp. 514-522, 1987.
[16] Arenas, J., Narbon, J.J., Alia, C., Optimum adhesive thickness in structural adhesives joints using statistical techniques based on Weibull distribution, International Journal of Adhesion & Adhesives, Vol. 30, pp. 160-165, 2010.
[17] Afendi, M., Teramoto, T., Bakri, H.B., Strength prediction of epoxy adhesively bonded scarf joints of dissimilar adherends, International Journal of Adhesion & Adhesives, Vol. 31, pp. 402-411, 2011.
[18] Hunston, D., Miyagi, Z., Schultheisz, C., Zaghi, S., The sandwich bending specimen for characterizing adhesive properties, Mechanics of Time-Dependent Materials, Vol. 7, pp. 71-88, 2003.
[19] Neves, A.A., Courinho, E., Poitevin, A., Influence of joint component mechanical properties and adhesive layer thickness on stress distribution in micro-tensile bond strength specimens, Dental Materials, Vol. 25, pp. 4-12, 2009.
[20] Noda, N.A., Miyazaki, T., Uchikoba, T., Li, R., Sano, Y., Takase, Y., Convenient Debonding Strength Evaluation Based on the Intensity of Singular Stress for Adhesive Joints. Transactions of The Japan Institute of Electronics Packaging, vol. 17, no. 2, pp. 132-142, 2014 (in Japanese).
[21] Dundurs, J., Discussion of edge-bonded dissimilar orthotropic elastic wedges under normal and shear loading. Trans ASME, J Appl Mech, Vol.36, pp.650-652, 1969.
[22] Bogy, D.B., Edge-Bonded Dissimilar Orthogonal Elastic Wedges under Normal and Shear Loading, Journal of Applied Mechanics, Vol. 35, pp. 460-466, 1968.
[23] Bogy, D.B., Two Edge-Bonded Elastic Wedges of Different and Wedge Angles under Surface Tractions, Journal of Applied Mechanics, Vol. 38, pp. 377-386, 1971.
[24] Miyazaki, T., Noda, N.A., Ren, F., Wang, Z., Sano, Y., Iida, K., Analysis of intensity of singular stress field for bonded cylinder and bonded pipe in comparison with bonded plate, International Journal of Adhesion and Adhesives, Vol. 77, pp 118-137, 2017.

[25] Timoshenko, S.P., Goodier,J.N., Theory of elasticity. Third Edition NewYork: McGrawHill, p. 380, 1970.

[26] Li, Y.L., Hu, S.Y., Munz, D., Yang, Y.Y., Asymptotic description of the stress field around the bond edge of a cylindrical joint, Archive of Applied Mechanics, Vol. 68, No. 7-8, pp. 552 -565, 1998.

[27] Hu, Q., Sato, Y., Watanabe, K., Dependence of stress state on elastic constants in axisymmetric dissimilar materials. Trans Jpn Soc Mech Eng Ser A, Vol.65, No.633, pp.1010-1017, 1999. [in Japanese].

[28] Hu, Q., Watanabe, K., A study on fundamental properties of elastic parameters related to stress field for dissimilar materials. Trans Jpn Soc Mech Eng Ser A, Vol.69, No.679, pp.594-601, 2003. [in Japanese].

[29] Yuuki, R., Mechanics of Interface, first ed. Baifuukann, Tokyo, 1992 (in Japanese).

[30] Naito, K., Onta, M., Kogo, Y., The effect of adhesive thickness on tensile and shear strength of polyimide adhesive, International Journal of Adhesion and Adhesives, Vol. 36, pp. 77 -85, 2012.

[31] Carpenter, W.C., Byers, C.A., path independent integral for computing stress intensities for V-notched cracks in a bi-material. Int J Fract, Vol.35, pp.245-268, 1978.